Fixed-Time Fuzzy Vibration Reduction for Stochastic MEMS Gyroscopes with Low Communication Resources

Yu Xia, Ke Xiao, Yangang Yao, Zhibo Geng and Zsófia Lendek

***Abstract*—The microelectromechanical system (MEMS) gyroscope is a complex nonlinear system with multiple variables, strong coupling, and susceptibility to stochastic disturbances. This paper presents an adaptive fuzzy control scheme for stochastic MEMS gyroscopes, with the primary objectives of reducing control vibration and achieving high precision prescribed performance tracking with low communication resources within a fixed-time backstepping framework. To address the stochastic disturbances and unknown nonlinear system dynamics, the interval type-3 fuzzy logic system (IT3FLS) is introduced. Additionally, a novel quadratic prescribed performance function (QPPF) is proposed to ensure satisfactory transient and steady-state performance of the system while mitigating initial control vibrations during fast error convergence. Furthermore, an event-triggered mechanism (ETM) is developed using a switching threshold strategy to minimize the communication load without compromising control accuracy. By utilizing the fixed-time command-filtered backstepping design method and newly introduced error-compensating signals, the issue of "explosion of complexity" is effectively resolved, and filtering errors are adequately compensated. The proposed control scheme guarantees that the tracking errors converge to a predefined set of arbitrarily small residuals in probability. In addition, all the closed-loop signals are within a fixed time bounded in probability (FTBIP). The simulation results validate the effectiveness and superiority of the proposed scheme.**

***Index Terms*—Adaptive prescribed fuzzy control, fixed-time stability, vibration reduction, low communication resources, stochastic MEMS gyroscope.**

I. Introduction

THE microelectromechanical system (MEMS) gyroscope is extensively used as an inertial device for measuring angular rates. It is strongly preferred in automotive applications, aerospace applications, consumer electronics, and mobile robotics due to its cost-effectiveness, low power consumption, and compactness[1]–[3]. However, certain unavoidable factors severely impact the MEMS gyroscope's tracking performance, during both transient and steady-state stages. These factors include variations in system parameters caused by fabrication imperfections [4] and stochastic disturbances [5] arising from practical operating environments. These challenges hinder the MEMS gyroscope from achieving high-performance measurement capabilities.

Currently, research is being conducted on the adaptive control of the MEMS gyroscope using both type-1 [6], [7] and type-2 [8], [9] fuzzy logic systems (FLSs) to effectively handle uncertain nonlinear functions. The significant role that type-1 and type-2 FLSs play in uncertainty modeling has prompted researchers to further extend them to higher types of fuzzy sets, particularly interval type-3 fuzzy sets. This concept has been explored and theorized in [10], [11], and it has been implemented in studies [12]–[16]. Meanwhile, the superiority of interval type-3 fuzzy logic systems (IT3FLSs) has been demonstrated through comparisons with type-1 and type-2 FLSs in these applications [12]–[16]. Unlike type-1 and type-2 FLSs that represent membership functions (MFs) using crisp values and type-1 fuzzy sets, respectively, IT3FLSs define MFs as a type-2 fuzzy set. The additional degrees of freedom enable IT3FLSs to effectively handle higher levels of uncertainties. However, the application of IT3FLS in stochastic nonlinear systems has not been explored yet. Therefore, comparing its ability to handle stochastic disturbances with that of type-1 and type-2 FLSs continues to be an intriguing and challenging area of research.

The previously discussed methods [6]–[16] have an infinite settling time, which makes them unsuitable for practical applications. To address this issue, the concept of finite-time stability was introduced [17], resulting in the exploration and development of various finite-time control schemes for stochastic systems [18]–[21]. However, existing finite-time control approaches have the drawback that the settling time is influenced by the initial system value, requiring repeated parameter adjustments to achieve the desired convergence time. To overcome this limitation, the fixed-time stability theorem (FTST) has been proposed in [22], ensure that the settling time solely depends on the system parameters. Consequently, numerous schemes based on the FTST have been developed for stochastic systems [23]–[26]. However, existing research on control of the MEMS gyroscope [2]–[9] has been primarily

The work was supported in part by the National Natural Science Foundation of China under Grant 52375039, in part by the National Key Research and Development Program of China under Grant 2022YFB4702201, and in part by the project DECIDE, no. 57/14.11.2022 funded under the PNRR I8 scheme by the Romanian Ministry of Research, Innovation, and Digitisation. *(Corresponding author: Ke Xiao and Zsófia Lendek.)*

Yu Xia and Ke Xiao are with the State Key Laboratory of Mechanical Transmission for Advanced Equipment, Chongqing University, Chongqing 400044, China (e-mails: 20132436@cqu.edu.cn; xiaoke993@cqu.edu.cn).

Yangang Yao is with the School of Information and Artificial Intelligence, Anhui Agricultural University, Hefei 230036, China, and also with the Department of Automation, University of Science and Technology of China, Hefei 230027, China (e-mail: ygyao@ustc.edu.cn).

Zhibo Geng is with College of Aeronautics and Astronautics, University of Electronic Science and Technology of China, Chengdu, Sichuan 611731, China (e-mail: gzbgeng@uestc.edu.cn).

Zsófia Lendek is with the Department of Automation, Technical University of Cluj-Napoca; Memorandumului 28, 400114, Cluj-Napoca, Romania, (e-mail: zsofia.lendek@aut.utcluj.ro).

based on deterministic models and overlooked the impact of stochastic disturbances. Additionally, the critical aspect of settling time has been neglected, rendering current approaches [2]–[9] unsuitable for practical applications. Thus, establishing a stochastic model of the MEMS gyroscope and designing a corresponding control scheme based on this stochastic model while considering settling time remains a challenging problem.

Since practical tracking control (PTC) of the MEMS gyroscope is more widely applicable and requires less restrictive constraints than asymptotic tracking control, it is the focus of many existing control methods. In PTC, achieving high tracking accuracy is of significant importance. As a result, research on schemes that emphasize predefined tracking accuracy has gained considerable attention, resulting in the proposal of numerous effective methods [4], [19], [27]–[36]. The initial introduction of the prescribed performance control (PPC) scheme in [27] has proven to be highly effective. Subsequently, the PPC technique has been applied to the MEMS gyroscope with different control strategies [4], [28]–[33]. However, a significant challenge that cannot be ignored is that the PPC for the MEMS gyroscope often requires a fast convergence rate, which can result in relatively large control torque vibrations in the initial stage. This vibration phenomenon can potentially damage the control system. Hence, the challenge we focus on is developing a vibration reduction PPC scheme tailored explicitly for the MEMS gyroscope, to mitigate this issue and enhance the overall performance.

Another limitation in current research on the MEMS gyroscope is the unnecessary resource usage that is commonly demanded. In many cases, electrostatic actuators and communication channels connecting the controller module and the actuator are activated at every sampling instant, even when the system is operating satisfactorily without requiring additional control actions. This results in the wastage of resources and significantly reduces the effective operational time of the MEMS gyroscope. To address this issue, the event-triggered mechanism (ETM) has been extensively studied in various applications [18], [20], [26], [28], [37]. It should be noted that the ETM only activates the actuators when preassigned conditions related to the system properties are violated, providing an effective solution to mitigating unnecessary resource usage. However, setting a large sampling interval fails to capture fast dynamics caused by unknown disturbances or abrupt reference changes, which can result in substantial tracking errors. Thus, the trade-off between tracking accuracy and communication resource utilization in the MEMS gyroscope continues to pose a challenge.

The control schemes mentioned above with the ETM are primarily designed within the backstepping framework, which encounters the challenge of "explosion of complexity." Fortunately, the issue has been addressed by recent studies [38], [39] through the introduction of command filter technology. This approach adeptly handles a range of nonlinear control challenges within the command filter-based backstepping design (CFBBD) framework. In [40], a controller was developed by integrating the adaptive technique with the CFBBD to achieve asymptotic tracking of uncertain nonlinear systems with time-varying parameters and disturbances. Moreover, an error compensation mechanism (ECM) was introduced in [41] to compensate for any errors introduced by the filter. A similar ECM was also discussed in [42], where a novel command filter was used to enhance filtering performance. As far as we are aware, there is no existing literature exploring CFBBD for the MEMS gyroscope. Give the above exposed challenges, we propose a control strategy for the MEMS gyroscope that has the following four contributions:

1) This study presents a stochastic model of the MEMS gyroscope, considering the influence of stochastic disturbances in controller design. The objective is to address the inherent challenge of the MEMS gyroscope accuracy being susceptible to stochastic disturbances, a topic that has not been previously explored in existing research [2]–[9], [28]–[30], [32], [33] on MEMS gyroscope control.
2) This study employs adaptive IT3FLS to handle the problem of stochastic disturbances for the first time. By comparing it with control strategies based on type-1 and type-2 FLSs, this study aims to demonstrate the potential of expanding the application of IT3FLS to solve more complex nonlinear control problems. Hence, the findings of this study hold significant implications for the advancement of fuzzy systems and their practical applications.
3) This study proposes a novel quadratic prescribed performance function (QPPF) for the first time. Compared with the traditional prescribed performance function (TPPF) [4], [19], [27]–[29], [31]–[33], the QPPF can guarantee a predefined tracking error while simultaneously reducing initial control vibrations, especially with fast error convergence rates. Moreover, the QPPF provides a feasible approach that can be generalized to other control systems [43]–[46] to minimize vibration damage while achieving the required tracking accuracy for certain urgent tasks.
4) This study ensures practical fixed-time tracking performance for the MEMS gyroscope by predefining the desired tracking errors, distinguishing it from existing control schemes [2]–[9], [28]–[30], [32], [33]. Moreover, in order to address the issue of complexity explosion and offset filtering errors, a novel ECM is introduced in conjunction with the CFBBD framework. Furthermore, the significance of the switching threshold event-triggered mechanism (STETM) in improving the communication resource limitations of the MEMS gyroscope is emphasized in our findings.

II. SYSTEM FORMULATION AND PRELIMINARIES

In this section, we will provide a detailed explanation of the derivation process of the stochastic MEMS gyroscope equation. Additionally, we will introduce the theoretical principles of the QPPF and the IT3FLS, while also covering the mathematical knowledge necessary for the controller design process.

TABLE I
SYSTEM PARAMETERS.

Notation	Explanation
m	weight of a proof mass
Ω_z^*	angular velocity
x^*, y^*	coordinates in drive and sensitive shaft
u_x^*, u_y^*	control inputs in drive and sensitive shafts
k_{xx}^*, k_{yy}^*	spring coefficients in drive and sensitive shafts
d_{xx}^*, d_{yy}^*	damping coefficients in drive and sensitive shafts
k_{xy}^*	coupled spring coefficient caused by asymmetric structure
d_{xy}^*	coupled damping coefficient caused by asymmetric structure

A. Dynamics of stochastic MEMS gyroscopes

Fig. 1 depicts the components of a typical MEMS gyroscope, which include a vibrational proof mass, a rigid frame, springs, and dampers. The rigid frame rotates around the rotation axis, while the control input torque induces oscillations in the vibrational proof mass along the drive axis. This oscillation generates a Coriolis force along the sense axis, allowing for the demodulation of the angular rate of the MEMS gyroscope. Some notations used are listed in Table I.

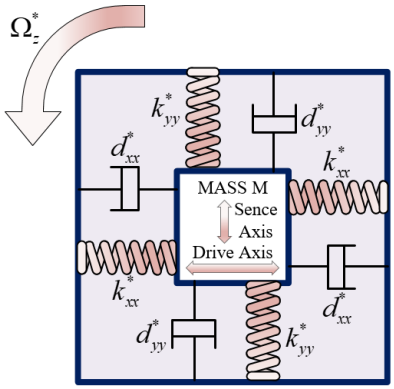

Fig. 1. Schematic of the MEMS gyroscope.

The standard dynamical model of the MEMS gyroscope [2]–[4] can be expressed as

$$\begin{aligned} m\ddot{x}^* + d_{xx}^*\dot{x}^* + d_{xy}^*\dot{y}^* + k_{xx}^*x^* + k_{xy}^*y^* &= u_x^* - 2m\Omega_z^*\dot{y}^*, \\ m\ddot{y}^* + d_{xy}^*\dot{x}^* + d_{yy}^*\dot{y}^* + k_{xy}^*x^* + k_{yy}^*y^* &= u_y^* - 2m\Omega_z^*\dot{x}^*. \end{aligned} \tag{1}$$

Non-dimensional processing of the dynamics (1) yields

$$\begin{aligned} \ddot{x} + d_{xx}\dot{x} + d_{xy}\dot{y} + \omega_x^2 x + \omega_{xy}y &= u_x - 2\Omega_z\dot{y}, \\ \ddot{y} + d_{xy}\dot{x} + d_{yy}\dot{y} + \omega_{xy}x + \omega_y^2 y &= u_y - 2\Omega_z\dot{x}, \end{aligned} \tag{2}$$

where $d_{ij} = d_{ij}^*/m\omega_0$, $\omega_i = \sqrt{k_{ii}^*/m\omega_0^2}$, $\omega_{ij} = k_{ij}^*/m\omega_0^2$, $x = x^*/q_0$, $\dot{x} = \dot{x}^*/\omega_0 q_0$, $\ddot{x} = \ddot{x}^*/\omega_0^2 q_0$, $y = y^*/q_0$, $\dot{y} = \dot{y}^*/\omega_0 q_0$, $\ddot{y} = \ddot{y}^*/\omega_0^2 q_0$, $u_i = u_i^*/m\omega_0^2 q_0$, m is the reference mass, q_0 denotes the length, and ω_0^2 indicates the resonance frequency. Indices $i = x$, $j = x$, and $i = y$, $j = y$ imply the coefficients in drive and sensitive shaft, respectively, $i = x$, $j = y$ means the coupled coefficient, and $\Omega_z = \Omega_z^*/\omega_0$ is the dimensionless angular velocity.

Considering the possibility of unknown variations in the damping and spring terms due to fabrication imperfections, the damping and spring coefficients in the non-dimensional expression above can be rewritten as $d_{ij}^* = d_{ij}^{*\mathrm{N}} + \Delta d_{ij}^*$ and $k_{ij}^* = k_{ij}^{*\mathrm{N}} + \Delta k_{ij}^*$, where $d_{ij}^{*\mathrm{N}}$ and $k_{ij}^{*\mathrm{N}}$ are the nominal terms, and Δd_{ij}^* and $\Delta k_{ij}^{*\mathrm{N}}$ are the unknown uncertainties. Accordingly, the non-dimensional terms are further derived as $d_{ij} = d_{ij}^{\mathrm{N}} + \Delta d_{ij}$, $\omega_i = \omega_i^{\mathrm{N}} + \Delta\omega_i$, $\omega_{ij} = \omega_{ij}^{\mathrm{N}} + \Delta\omega_{ij}$, where $d_{ij}^{\mathrm{N}} = d_{ij}^{*\mathrm{N}}/m\omega_0$, $\omega_i^{\mathrm{N}} = \sqrt{k_{ii}^{*\mathrm{N}}/m\omega_0^2}$, $\omega_{ij}^{\mathrm{N}} = k_{ij}^{*\mathrm{N}}/m\omega_0^2$, and $\Delta d_{ij} = \Delta d_{ij}^*/m\omega_0$, $\Delta\omega_i = \sqrt{\Delta k_{ii}^*/m\omega_0^2}$, $\Delta\omega_{ij} = \Delta k_{ij}^*/m\omega_0^2$.

Then, the compound nonlinearities of the dynamics are defined as

$$\begin{aligned} \bar{f}_1 &= -d_{xx}\dot{x} - (d_{xy} - 2\Omega_z)\,\dot{y} - \omega_x^2 x - \omega_{xy}y, \\ \bar{f}_2 &= -(d_{xy} + 2\Omega_z)\,\dot{x} - d_{yy}\dot{y} - \omega_{xy}x - \omega_y^2 y. \end{aligned} \tag{3}$$

With (3), and denoting $x_1 = x$, $x_2 = \dot{x}$, $x_3 = y$, and $x_4 = \dot{y}$, dynamics (2) can be rewritten as

$$\begin{cases} \dot{x}_1 = x_2, \\ \dot{x}_2 = \bar{f}_1 + u_x, \\ \dot{x}_3 = x_4, \\ \dot{x}_4 = \bar{f}_2 + u_y. \end{cases} \tag{4}$$

In practical applications, the MEMS gyroscope is susceptible to stochastic disturbances, which can significantly impact system performance. Considering the form of stochastic nonlinear systems [19] as $d\chi = F(\chi)\,dt + G^T(\chi)\,d\omega$, we can extend the dimensionless model (4) to a stochastic dynamic model as follows:

$$\begin{cases} dx_1 = (x_2 + f_1(x))\,dt + G_1^T(x)\,dw, \\ dx_2 = (u_x + f_2(x))\,dt + G_2^T(x)\,dw, \\ dx_3 = (x_4 + f_3(x))\,dt + G_3^T(x)\,dw, \\ dx_4 = (u_y + f_4(x))\,dt + G_4^T(x)\,dw, \end{cases} \tag{5}$$

where $x = [x_1, x_2, x_3, x_4] = [x, \dot{x}, y, \dot{y}]$ indicates the system state vector, ω denotes a standard Brownian motion, $f_i(x)$ and $G_i^T(x)$, $i = 1, 2, 3, 4$ are the unknown continuous functions, and $f_i = [f_1, f_2, f_3, f_4] = \left[0, \bar{f}_1, 0, \bar{f}_2\right]$.

Control Goal: Develop an adaptive control scheme for the stochastic MEMS gyroscope (5) in which all the signals are ensured to be FTBIP and the residual errors are guaranteed to be in prescribed performance bounds.

Remark 1: When stochastic disturbances are encountered, the control performance and stability of the overall closed-loop system can be compromised, which is the primary motivation for considering stochastic control of the MEMS gyroscope.

B. Quadratic Prescribed Performance Function

First, we define the tracking errors of the MEMS gyroscope as follows:

$$e_i(t) = x_i(t) - x_i^d(t), \tag{6}$$

where x_i^d, $i = 1, 3$ denote the reference signals.

To characterize the vibration reduction tracking performance of the system within the predefined behavior function, we propose the QPPF

$$\rho_i(t) = (\rho_{i0} - \rho_{i\infty})\,e^{-\ell_i t^2} + \rho_{i\infty}, \tag{7}$$

where ρ_{i0} and $\rho_{i\infty}, i = 1, 3$ represent the expected upper bounds for the initial and steady-state tracking errors, respectively. Terms $\ell_i, i = 1, 3$ reflect the convergence rate of

$\rho_i(t)$, which gradually decay to a final value of $\rho_{i\infty}$ as time approaches infinity. Moreover, $\rho_i(t), i = 1, 3$ satisfy the initial condition $-\rho_i(0) < e_i(0) < \rho_i(0)$.

Then, we define the converted tracking errors as follows:

$$s_i(t) = \tan\left(\frac{\pi e_i(t)}{2\rho_i(t)}\right), e_i(0) < \rho_i(0), \tag{8}$$

where $s_i(t), i = 1, 3$ are the transformed tracking errors, and their time derivatives can be deduced as

$$ds_i(t) = \lambda_i\left(dx_i - \dot{x}_i^d - \frac{2}{\pi}\dot{\rho}_i(t)\arctan(s_i(t))\right), \tag{9}$$

where $\lambda_i = \pi\left(1 + s_i^2(t)\right)/2\rho_i(t), i = 1, 3$.

Remark 2: From a practical engineering perspective, it is important to select significant convergence rates ℓ_i to ensure that the system response of the MEMS gyroscope can effectively meet the requirements of the majority of measurement tasks.

Remark 3: Based on current research [4], [19], [27]–[29], [31]–[33] where the TPPF is typically designed as $\rho_i(t) = (\rho_{i0} - \rho_{i\infty})e^{-\ell_i t} + \rho_{i\infty}$, the following represents the design of the corresponding universal control law:
$u_i = \lambda_i{}^{-1}\left(-k_i s_i(t) + \frac{\lambda_i e_i(t)\dot{\rho}_i(t)}{\rho_i(t)}\right) + \dot{x}_i^d$.
This indicates that considerable convergence rates ℓ_i cause initial rapid fluctuations of $\dot{\rho}_i$. Accordingly, significant vibrations of the inputs $u_i, i = 1, 3$ during the initial phase are unavoidable.

Remark 4: The design of the QPPF is inspired by the quadratic characteristics of the normal distribution curve. The design idea is to create a performance function that exhibits a gentler decline than the TPPF at the outset, then drops at a rate similar to the TPPF in the middle of the decline, and maintains the same limiting boundary as TPPF at the end of the decline. In other words, the slope of the QPPF will be smaller than that of the TPPF at the initial stage of decline, resulting in a smaller derivative of the QPPF during this phase. As discussed in Remark 3, the control input required by the QPPF will also be smaller.

Remark 5: In contrast with the TPPF, the QPPF proposed in this paper is capable of smoothly transitioning the exponential boundary in the early stages of convergence, thereby helping to reduce vibrations of u_i. However, it is important to note that this relatively smooth decline may trade off with the convergence speed. Therefore, when utilizing the QPPF, it becomes crucial to select the design parameters (ρ_{i0}, $\rho_{i\infty}$, ℓ_i) more judiciously to align with the specific requirements of the application. A comparison of the two behavioural functions is depicted in Fig. 2 ($\ell_i = 1, \ell_i = 10$).

C. Interval type-3 fuzzy logic system

As demonstrated in [47], the IT3FLS possesses superior uncertainty modeling capabilities, increased disturbance resistance, and a reduced number of membership functions in comparison to type-2/type-1 FLSs. Consequently, IT3FLS is employed to approximate the unknown nonlinear functions with stochastic disturbances in this paper.

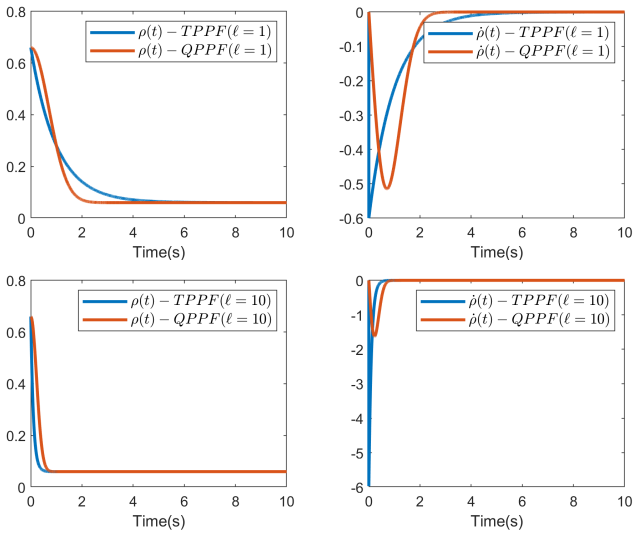

Fig. 2. Behavior of TPPF and QPPF.

Consider $\tilde{\xi}_i^j$ as the j-th fuzzy sets for the inputs $X_i, i = 1, \ldots, n$, the memberships at secondary levels M_{1i} and M_{2i} are given as

$$U_{1|\tilde{\xi}_i^j|M_{1i}} = \begin{cases} 1 - \left(\left|X_i - \Gamma_{\tilde{\xi}_i^j}\right| / \theta_{2|\tilde{\xi}_i^j}\right)^{M_{1i}}, \\ \text{if} \Gamma_{\tilde{\xi}_i^j} - \theta_{2|\tilde{\xi}_i^j} < X_i \le \Gamma_{\tilde{\xi}_i^j} \\ 0, \text{if} X_i > \Gamma_{\tilde{\xi}_i^j} + \theta_{1|\tilde{\xi}_i^j} \text{or} X_i \le \Gamma_{\tilde{\xi}_i^j} - \theta_{2|\tilde{\xi}_i^j} \\ 1 - \left(\left|X_i - \Gamma_{\tilde{\xi}_i^j}\right| / \theta_{1|\tilde{\xi}_i^j}\right)^{M_{1i}}, \\ \text{if} \Gamma_{\tilde{\xi}_i^j} < X_i \le \Gamma_{\tilde{\xi}_i^j} + \theta_{1|\tilde{\xi}_i^j} \end{cases},$$

$$U_{1|\tilde{\xi}_i^j|M_{2i}} = \begin{cases} 1 - \left(\left|X_i - \Gamma_{\tilde{\xi}_i^j}\right| / \theta_{2|\tilde{\xi}_i^j}\right)^{M_{2i}}, \\ \text{if} \Gamma_{\tilde{\xi}_i^j} - \theta_{2|\tilde{\xi}_i^j} < X_i \le \Gamma_{\tilde{\xi}_i^j} \\ 0, \text{if} X_i > \Gamma_{\tilde{\xi}_i^j} + \theta_{1|\tilde{\xi}_i^j} \text{or} X_i \le \Gamma_{\tilde{\xi}_i^j} - \theta_{2|\tilde{\xi}_i^j} \\ 1 - \left(\left|X_i - \Gamma_{\tilde{\xi}_i^j}\right| / \theta_{1|\tilde{\xi}_i^j}\right)^{M_{2i}}, \\ \text{if} \Gamma_{\tilde{\xi}_i^j} < X_i \le \Gamma_{\tilde{\xi}_i^j} + \theta_{1|\tilde{\xi}_i^j} \end{cases},$$

$$U_{2|\tilde{\xi}_i^j|M_{1i}} = \begin{cases} 1 - \left(\left|X_i - \Gamma_{\tilde{\xi}_i^j}\right| / \theta_{2|\tilde{\xi}_i^j}\right)^{1/M_{1i}}, \\ \text{if} \Gamma_{\tilde{\xi}_i^j} - \theta_{2|\tilde{\xi}_i^j} < X_i \le \Gamma_{\tilde{\xi}_i^j} \\ 0, \text{if} X_i > \Gamma_{\tilde{\xi}_i^j} + \theta_{1|\tilde{\xi}_i^j} \text{or} X_i \le \Gamma_{\tilde{\xi}_i^j} - \theta_{2|\tilde{\xi}_i^j} \\ 1 - \left(\left|X_i - \Gamma_{\tilde{\xi}_i^j}\right| / \theta_{1|\tilde{\xi}_i^j}\right)^{1/M_{1i}}, \\ \text{if} \Gamma_{\tilde{\xi}_i^j} < X_i \le \Gamma_{\tilde{\xi}_i^j} + \theta_{1|\tilde{\xi}_i^j} \end{cases},$$

$$U_{2|\tilde{\xi}_i^j|M_{2i}} = \begin{cases} 1 - \left(\left|X_i - \Gamma_{\tilde{\xi}_i^j}\right| / \theta_{2|\tilde{\xi}_i^j}\right)^{1/M_{2i}}, \\ \text{if} \Gamma_{\tilde{\xi}_i^j} - \theta_{2|\tilde{\xi}_i^j} < X_i \le \Gamma_{\tilde{\xi}_i^j} \\ 0, \text{if} X_i > \Gamma_{\tilde{\xi}_i^j} + \theta_{1|\tilde{\xi}_i^j} \text{or} X_i \le \Gamma_{\tilde{\xi}_i^j} - \theta_{2|\tilde{\xi}_i^j} \\ 1 - \left(\left|X_i - \Gamma_{\tilde{\xi}_i^j}\right| / \theta_{1|\tilde{\xi}_i^j}\right)^{1/M_{2i}}, \\ \text{if} \Gamma_{\tilde{\xi}_i^j} < X_i \le \Gamma_{\tilde{\xi}_i^j} + \theta_{1|\tilde{\xi}_i^j} \end{cases}, \tag{10}$$

where $U_{1|\tilde{\xi}_i^j|M_{2i}}$ / $U_{1|\tilde{\xi}_i^j|M_{2i}}$ and $U_{2|\tilde{\xi}_i^j|M_{1i}}$ / $U_{2|\tilde{\xi}_i^j|M_{2i}}$ are the upper/lower memberships for $\tilde{\xi}_i^j$ at M_{2i} and M_{1i}. Terms $\theta_{2|\tilde{\xi}_i^j}$ and $\theta_{1|\tilde{\xi}_i^j}$ are the distances from the centre $\Gamma_{\tilde{\xi}_i^j}$ to the start/end points of $\tilde{\xi}_i^j$.

The rule firings are

$$\begin{aligned}\vartheta^l_{1|M_{1i}}&=\prod_{j=1}^{n}U_{1|\tilde{\xi}_i^j|M_{1i}},\vartheta^l_{1|M_{2i}}=\prod_{j=1}^{n}U_{1|\tilde{\xi}_i^j|M_{2i}},\\ \vartheta^l_{2|M_{1i}}&=\prod_{j=1}^{n}U_{2|\tilde{\xi}_i^j|M_{1i}},\vartheta^l_{2|M_{2i}}=\prod_{j=1}^{n}U_{2|\tilde{\xi}_i^j|M_{2i}},\end{aligned}\tag{11}$$

where the $l-\text{th}$ IF-THEN rule is: IF X_1 is $\tilde{\xi}_1^{P1}$ and $\cdots$ and X_n is $\tilde{\xi}_1^{Pn}$, THEN $\mu\in[\psi_{2l},\psi_{1l}]$, $l=1,2,\ldots,\varpi$, where $\tilde{\xi}_i^{Pj}$ is the $Pj-\text{th}$ fuzzy sets for X_i, and ψ_{2l} and ψ_{1l} are consequent parameters.

Then, we can obtain

$$\mu=\frac{\sum_{i=1}^{n_M}\left(M_{2i}\mu_{2i}+M_{1i}\mu_{1i}\right)}{\sum_{i=1}^{n_M}\left(M_{2i}+M_{1i}\right)},\tag{12}$$

where

$$\mu_{1i}=\frac{\sum_{i=1}^{n_r}\left(\xi^l_{1|M_{1i}}\psi_{1l}+\xi^l_{2|M_{1i}}\psi_{2l}\right)}{\sum_{i=1}^{n_r}\left(\xi^l_{1|M_{1i}}+\xi^l_{2|M_{1i}}\right)},$$

$$\mu_{2i}=\frac{\sum_{i=1}^{n_r}\left(\xi^l_{1|M_{2i}}\psi_{1l}+\xi^l_{2|M_{2i}}\psi_{2l}\right)}{\sum_{i=1}^{n_r}\left(\xi^l_{1|M_{2i}}+\xi^l_{2|M_{2i}}\right)}.$$

Now, the output $Y(X)$ can be written as

$$Y(X)=\psi^T H(X),\tag{13}$$

where

$$\psi^T=[\psi_{21},\ldots,\psi_{2nr},\psi_{11},\ldots,\psi_{1nr}],$$

$$H=[H_{21},\ldots,H_{2nr},H_{11},\ldots,H_{1nr}],$$

$$H_{2l}=\frac{\sum\limits_{i=1}^{n_M}M_{2i}\vartheta^l_{2|M_{2i}}}{\sum\limits_{i=1}^{n_M}(M_{2i}+M_{1i})\sum\limits_{l=1}^{n_r}\left(\vartheta^l_{1|M_{2i}}+\vartheta^l_{2|M_{2i}}\right)}+\frac{\sum\limits_{i=1}^{n_M}M_{1i}\vartheta^l_{2|M_{1i}}}{\sum\limits_{i=1}^{n_M}(M_{2i}+M_{1i})\sum\limits_{l=1}^{n_r}\left(\vartheta^l_{1|M_{1i}}+\vartheta^l_{2|M_{1i}}\right)},$$

$$H_{1l}=\frac{\sum\limits_{i=1}^{n_M}M_{2i}\vartheta^l_{1|M_{2i}}}{\sum\limits_{i=1}^{n_M}(M_{2i}+M_{1i})\sum\limits_{l=1}^{n_r}\left(\vartheta^l_{1|M_{2i}}+\vartheta^l_{2|M_{2i}}\right)}+\frac{\sum\limits_{i=1}^{n_M}M_{1i}\vartheta^l_{1|M_{1i}}}{\sum\limits_{i=1}^{n_M}(M_{2i}+M_{1i})\sum\limits_{l=1}^{n_r}\left(\vartheta^l_{1|M_{1i}}+\vartheta^l_{2|M_{1i}}\right)}.$$

Lemma 1 [18]: For an unknown nonlinear function $F(X)$ defined on a compact set Ω, and any $\varepsilon\in R^+$, there is a FLS (13) such that

$$\sup_{X\in\Omega}\left|F(X)-\psi^T H(X)\right|\le\varepsilon.\tag{14}$$

D. Preliminaries

Definition 1 [19]: Consider the stochastic system:

$$d\chi=F(\chi)\,dt+G^T(\chi)\,d\omega.\tag{15}$$

Define the following differential operator $\mathcal{L}$ of the positive definite function $V(\chi)$:

$$\mathcal{L}V(\chi)=\frac{\partial V}{\partial\chi}F(\chi)+\frac{1}{2}Tr\left\{G^T(\chi)\frac{\partial^2 V}{\partial\chi^2}G(\chi)\right\}.\tag{16}$$

Lemma 2 [23]: If there exist two functions $\Lambda_1(\cdot),\Lambda_2(\cdot)\in k_\infty$, and some constants $\sigma_1,\sigma_2,\beta>0$, $0<p<1$, $q>1$ such that

$$\begin{aligned}&\Lambda_1(\|\chi\|)\le V(\chi)\le\Lambda_2(\|\chi\|),\\ &\mathcal{L}V(\chi)\le-\sigma_1V^p(\chi)-\sigma_2V^q(\chi)+\beta,\end{aligned}\tag{17}$$

then, the solution of (15) is FTBIP for any $0<\eta<1$ with

$$E[T]\le T_s=\frac{1}{\sigma_1\eta(1-p)}+\frac{1}{\sigma_2\eta(q-1)}.\tag{18}$$

Lemma 3 [50]: Consider the following filter:

$$\begin{cases}\dot\varphi_{11}=\varphi_{12}-r_{11}M^{\frac{1}{2}}\text{sig}(\varphi_{11}-\alpha_1)^{\frac{1}{2}}\\ \qquad\quad-h_{11}N^{\frac{1}{2}}\text{sig}(\varphi_{11}-\alpha_1)^{\mu_{11}},\\ \dot\varphi_{12}=-r_{12}M\text{sig}(\varphi_{12}-\dot\varphi_{11})-h_{12}N\text{sig}(\varphi_{11}-\alpha_i)^{\mu_{12}},\end{cases}\tag{19}$$

where $\text{sig}^\alpha=|\cdot|^\alpha\text{sign}(\cdot)$, $\mu_{1i}=i\mu-(i-1)$, where $\mu\in(1,1+\iota)$ with sufficiently small $\iota>0$, $M,N>0$, r_{i1}, r_{i2}, h_{i1}, h_{i2} are selected so that the matrices $A_1=\begin{bmatrix}-r_{i1}&1\\-r_{i2}&0\end{bmatrix}$ and $A_2=\begin{bmatrix}-h_{i1}&1\\-h_{i2}&0\end{bmatrix}$ are Hurwitz. Then, the output of (19) satisfies $\bar\alpha_1=\varphi_{11}$, $\dot{\bar\alpha}_1=\dot\varphi_{11}$, and $\bar\alpha_1-\alpha_1\le\eta$ within a fixed time T_F, where η is a design constant and T_F can be expressed as

$$E[T]\le T_F=\frac{2\lambda_{\max}^{\frac{3}{2}}(P_1)}{\lambda_{\min}(Q_1)}+\frac{\lambda_{\max}(P_2)}{\lambda_{\min}(Q_2)(\mu-1)\varsigma^{\mu-1}},\tag{20}$$

where $\varsigma\le\lambda_{\min}(P_2)$, and P_1, P_2, Q_1, and Q_2 satisfy

$$\begin{aligned}P_1A_1+A_1^TP_1&=-Q_1,\\ P_2A_2+A_2^TP_2&=-Q_2.\end{aligned}\tag{21}$$

Lemma 4 [42]: For any $x,y\in R$, $a_1,a_2,a_3\in R^+$, it holds that

$$|x|^{a_1}|y|^{a_2}\le\frac{a_1}{a_1+a_2}a_3|x|^{a_1+a_2}+\frac{a_1}{a_1+a_2}a^{-\frac{a_1}{a_2}}|y|^{a_1+a_2}.\tag{22}$$

Lemma 5 [26]: For any $x\in R$ and $y\in R^+$, one has

$$0\le|x|-\frac{2}{\pi}x\tanh\left(\frac{x}{\wp}\right)\le\frac{2}{\pi}y.\tag{23}$$

Lemma 6 [26]: For any $0<\varsigma<1$ and $x_i\in R$, $i=1,\ldots,n$, one has

$$\left(\sum_{i=1}^{n}|x_i|\right)^2\le n\sum_{i=1}^{n}x_i^2,\left(\sum_{i=1}^{n}|x_i|\right)^\varsigma\le\sum_{i=1}^{n}|x_i|^\varsigma.\tag{24}$$

Assumption 1: The reference signals x_i^d, $i=1,3$ and their derivatives $\dot x_i^d$ are continuous and bounded.

Remark 6: Assumption 1 is essential for controlling system (5). It is important to note that unlike the traditional backstepping method [21], [23], which assumes the reference signal and its derivative are continuously differentiable up to the $(n+1)$th-order, this paper introduces the filters as in [20], [40], thus only requiring the continuity and boundedness of the reference signals x_i^d, $i=1,3$ and their first derivatives $\dot x_i^d$.

III. CONTROL DESIGN AND STABILITY ANALYSIS

In this section, we will present a detailed procedure for designing the command filter-based prescribed performance fixed-time event-triggered fuzzy vibration reduction controller for the stochastic MEMS gyroscope. The stability analysis, based on the fixed-time Lyapunov criterion, will also be included. Notably, the controller design incorporates the ECM and the IT3FLS to effectively handle filter errors and stochastic disturbances, thereby enhancing the overall performance of the controller. Additionally, with the aim of conserving communication resources, this section will also present the utilization of the STETM and examine its non-Zeno behaviour.

A. Control Design

Define the following error systems:

$$z_i(t) = \begin{cases} s_i(t), i = 1,3, \\ x_i(t) - \bar{\alpha}_i(t), i = 2,4, \end{cases} \tag{25}$$

where $\bar{\alpha}_i(t), i = 2,4$ are the outputs of the following filter:

$$\begin{cases} \dot{\varphi}_{i1} = \varphi_{i2} - r_{i1} M^{\frac{1}{2}} \mathrm{sig}(\varphi_{i1} - \alpha_i)^{\frac{1}{2}} \\ \qquad - h_{i1} N^{\frac{1}{2}} \mathrm{sig}(\varphi_{i1} - \alpha_i)^{\mu_{i1}}, \\ \dot{\varphi}_{i2} = -r_{i2} M \mathrm{sig}(\varphi_{i2} - \dot{\varphi}_{i1}) - h_{i2} N \mathrm{sig}(\varphi_{i1} - \alpha_i)^{\mu_{i2}}, \end{cases} \tag{26}$$

where $\bar{\alpha}_i = \varphi_{i1}$, $\dot{\bar{\alpha}}_i = \dot{\varphi}_{i1}$, and the meaning of the parameters is the same as in (19).

Subsequently, define the compensated error variables

$$v_i = z_i - \zeta_i, \tag{27}$$

where $\zeta_i, i = 1,2,3,4$ are compensation signals that will be specified in the i-th control design step.

Remark 7: The purpose of implementing ECM is to minimize the impact of filter error on the transient performance. It should be noted that the ECM was also utilized in [20] and [41], although these approaches only focused on ensuring the finite-time stability of the ECM. In contrast, the ECM proposed in this paper effectively compensates for filter errors and guarantees the stability of the ECM within a fixed time.

Step 1: Define the compensation signal ζ_1 as follows:

$$\dot{\zeta}_1 = -l_{11}{\zeta_1}^3 + \lambda_1(\bar{\alpha}_2 - \alpha_2) + \lambda_1\zeta_2 - \lambda_1 l_{12}\mathrm{sign}(\zeta_1), \tag{28}$$

where l_{11} and l_{12} are design parameters.

From (5), (6), (9), and (25)–(28), one has

$$\begin{aligned} dv_1 = \big(&\lambda_1\big(v_2 + \alpha_2 - \tfrac{2}{\pi}\dot{\rho}_1 \arctan(s_1) - \dot{x}_1^d \\ &+ l_{12}\mathrm{sign}(\zeta_1)\big) + l_{11}{\zeta_1}^3\big)\,dt + G_1^T dw. \end{aligned} \tag{29}$$

Select the first Lyapunov function candidate as follows:

$$V_1 = \frac{1}{4}v_1^4 + \frac{1}{2\gamma_1}\tilde{\Theta}_1^T\tilde{\Theta}_1, \tag{30}$$

where $\tilde{\Theta}_1 = \Theta_1 - \hat{\Theta}_1$ is the estimation error with the ideal value Θ_1 and the estimated value $\hat{\Theta}_1$, and γ_1 is a design parameter.

Based on Definition 1, one has

$$\begin{aligned} \mathcal{L}V_1 = \lambda_1 v_1^3\big(&v_2 + \alpha_2 - \tfrac{2}{\pi}\dot{\rho}_1\arctan(s_1) \\ &+ l_{12}\mathrm{sign}(\zeta_1) - \dot{x}_1^d\big) + l_{11}{\zeta_1}^3 v_1^3 \\ &+ \tfrac{3}{2}\lambda_1^2 v_1^2 G_1^T G_1 - \tfrac{1}{\gamma_1}\tilde{\Theta}_1\dot{\hat{\Theta}}_1. \end{aligned} \tag{31}$$

According to Lemma 4, one has

$$\frac{3}{2}\lambda_1^2 v_1^2 G_1^T G_1 \le \frac{3}{4}\lambda_1^4 v_1^4 \|G_1\|^4 + \frac{3}{4}. \tag{32}$$

Substituting (32) into (31) yields

$$\begin{aligned} \mathcal{L}V_1 \le \lambda_1 v_1^3\big(&v_2 + \alpha_2 - \tfrac{2}{\pi}\dot{\rho}_1\arctan(s_1) \\ &+ l_{12}\mathrm{sign}(\zeta_1) - \dot{x}_1^d + F_1(X_1)\big) \\ &- \tfrac{1}{\gamma_1}\tilde{\Theta}_1\dot{\hat{\Theta}}_1 + \tfrac{3}{4}, \end{aligned} \tag{33}$$

where $F_1(X_1) = 3\lambda_1^3 v_1 \|G_1\|^4/4 + l_{11}{\zeta_1}^3 v_1^3/\lambda_1$. The IT3FLS is introduced to approximate $F_1(X_1)$, i.e., $F_1(X_1) = \psi_1^T H_1(X_1) + \varepsilon_1(X_1)$. With Lemma 1, we assume that $|\varepsilon_1(X_1)| \le \varepsilon_{1M}$, where $\varepsilon_{1M} \in R^+$.

Define the following ideal parameter ψ_1:

$$\psi_1 = \arg\min_{\hat{\psi}_1 \in \Psi_1}\left[\sup_{X_1 \in \mathrm{X}_{X_1}}\left|\hat{\psi}_1 H_1(X_1) - F_1(X_1)\right|\right], \tag{34}$$

where Ψ_1 and X_1 are compact sets for $\hat{\psi}_1$ and X_1, and $\hat{\psi}_1$is the estimation of ψ_1. The subsequent steps involve calculating ideal weights similar to (34). However, they are not displayed in the following controller design process to save space. The interested reader is referred to [35], [41].

Based on Lemma 4 again, we can obtain

$$\begin{aligned} &\lambda_1 v_1^3 F_1(X_1) \le \tfrac{1}{2a_{11}}\lambda_1^2 v_1^6 \Theta_1 H_1^T H_1 + \tfrac{3}{4a_{12}} v_1^4 \lambda_1^{\frac{4}{3}} \\ &\qquad + \tfrac{2a_{11} + a_{12}^3 \varepsilon_{1M}^4}{4}, \\ &\lambda_1 v_1^3 l_{12}\mathrm{sign}(\zeta_1) \le \tfrac{3}{4a_{13}}\lambda_1^{\frac{4}{3}} v_1^4 + \tfrac{a_{13}^3}{4} l_{12}^4, \\ &\lambda_1 v_1^3 v_2 \le \tfrac{3}{4}\lambda_1^{\frac{4}{3}} v_1^4 + \tfrac{1}{4}v_2^4, \end{aligned} \tag{35}$$

where $a_{11}, a_{12}, a_{13} \in R^+$ are design constants, and $\Theta_1 = \max\|\psi_1\|^2$ is the learning parameter.

Substituting (35) into (33) yields

$$\begin{aligned} \mathcal{L}V_1 \le \lambda_1 v_1^3\big(&\alpha_2 - \tfrac{2}{\pi}\dot{\rho}_1\arctan(s_1) \\ &+ \tfrac{1}{2a_{11}}\lambda_1 v_1^3 \hat{\Theta}_1 H_1^T H_1 - \dot{x}_1^d + \tfrac{3}{4}\lambda_1^{\frac{1}{3}} v_1 \\ &+ \tfrac{3}{4a_{12}}\lambda_1^{\frac{1}{3}} v_1 + \tfrac{3}{4a_{13}}\lambda_1^{\frac{1}{3}} v_1\big) \\ &+ \tfrac{3 + 2a_{11} + a_{12}^3\varepsilon_{1M}^4 + a_{13}^3 l_{12}^4}{4} + \tfrac{1}{4}v_2^4 \\ &+ \tilde{\Theta}_1\left(-\tfrac{1}{\gamma_1}\dot{\hat{\Theta}}_1 + \tfrac{1}{2a_{11}}\lambda_1^2 v_1^6 H_1^T H_1\right). \end{aligned} \tag{36}$$

Design α_2 and $\hat{\Theta}_1$ for the first subsystem as follows:

$$\begin{aligned} \alpha_2 = &-k_{p1} v_1^{4p-3} - k_{q1} v_1^{4q-3} + \dot{x}_1^d \\ &+ \tfrac{2}{\pi}\dot{\rho}_1\arctan(s_1) - \tfrac{1}{2a_{11}}\lambda_1 v_1^3 \hat{\Theta}_1 H_1^T H_1 \\ &- \tfrac{3}{4}\lambda_1^{\frac{1}{3}} v_1 - \tfrac{3}{4a_{12}}\lambda_1^{\frac{1}{3}} v_1 - \tfrac{3}{4a_{13}}\lambda_1^{\frac{1}{3}} v_1, \end{aligned} \tag{37}$$

$$\dot{\hat{\Theta}}_1 = -\frac{\gamma_1}{2a_{11}}\lambda_1^2 v_1^6 H_1^T H_1 - p_{\Theta 11}\hat{\Theta}_1 - p_{\Theta 12}\hat{\Theta}_1^{2q-1}, \tag{38}$$

where $k_{p1}, k_{q1}, p_{\Theta 11}, p_{\Theta 12} \in R^+$ are design parameters.

Substituting (37) and (38) into (36) yields

$$\begin{aligned} &\mathcal{L}V_1 \le -k_{p1} v_1^{4p} - k_{q1} v_1^{4q} + \tfrac{1}{\gamma_1} p_{\Theta 11}\tilde{\Theta}_1\hat{\Theta}_1 \\ &+ \tfrac{1}{\gamma_1} p_{\Theta 12}\tilde{\Theta}_1\hat{\Theta}_1^{2q-1} + \tfrac{3 + 2a_{11} + a_{12}^3\varepsilon_{1M}^4 + a_{13}^3 l_{12}^4}{4} + \tfrac{1}{4}v_2^4. \end{aligned} \tag{39}$$

It should be noted that

$$\begin{aligned} &\tfrac{p_{\Theta 11}}{\gamma_1}\tilde{\Theta}_1\hat{\Theta}_1 \le \tfrac{p_{\Theta 11}}{2\gamma_1}\Theta_1^2 - \tfrac{p_{\Theta 11}}{2\gamma_1}\tilde{\Theta}_1^2, \\ &\left(\tilde{\Theta}_1^2\right)^p \le \tilde{\Theta}_1^2 + (1-p)\,p^{\frac{p}{1-p}}, \\ &\tfrac{p_{\Theta 12}}{\gamma_1}\tilde{\Theta}_1\hat{\Theta}_1^{2q-1} \le \tfrac{p_{\Theta 12}(2q-1)}{2q\gamma_1}\left(\Theta_1^{2q} - \tilde{\Theta}_1^{2q}\right). \end{aligned} \tag{40}$$

Then, the following can be obtained:

$$\begin{aligned}\mathcal{L}V_1 \leq & -k_{p1}v_1^{4p} - k_{q1}v_1^{4q} - \tfrac{p_{\Theta 11}}{2\gamma_1}\tilde{\Theta}_1^{2p} \\ & - \tfrac{p_{\Theta 12}(2q-1)}{2q\gamma_1}\tilde{\Theta}_1^{2q} + \tfrac{1}{4}v_2^4 + \Xi_1,\end{aligned} \tag{41}$$

where $\Xi_1 = p_{\Theta 11}\Theta_1^2/2\gamma_1 + (1-p)\,p_{\Theta 11}p^{p/(1-p)}/2\gamma_1 + \left(3 + 2a_{11} + a_{12}^3\varepsilon_{1M}^4 + a_{13}^3 l_{12}^4\right)/4 + (2q-1)\,p_{\Theta 12}\Theta_1^{2q}/2q\gamma_1$.

Step 2: Define the compensation signal ζ_2 as follows:

$$\dot{\zeta}_2 = -l_{21}{\zeta_2}^3 - \lambda_1\zeta_1 - l_{22}\mathrm{sign}\left(\zeta_2\right), \tag{42}$$

where l_{21} and l_{22} are design parameters.

From (5), (25)–(27), and (42), one has

$$\begin{aligned}dv_2 = & \left(u_x + f_2 - \dot{\bar{\alpha}}_2 + l_{21}{\zeta_2}^3 + \lambda_1\zeta_1\right. \\ & \left. + l_{22}\mathrm{sign}\left(\zeta_2\right)\right)dt + G_2^T dw.\end{aligned} \tag{43}$$

Select the second Lyapunov function candidate as follows:

$$V_2 = V_1 + \frac{1}{4}v_2^4 + \frac{1}{2\gamma_2}\tilde{\Theta}_2^T\tilde{\Theta}_2, \tag{44}$$

where $\tilde{\Theta}_2 = \Theta_2 - \hat{\Theta}_2$ is the estimation error with the ideal value Θ_2 and the estimated value $\hat{\Theta}_2$, and γ_2 is a design parameter.

From (41)–(44), one has

$$\begin{aligned}\mathcal{L}V_2 \leq & v_2^3\left(u_x + f_2 - \dot{\bar{\alpha}}_2 + l_{21}{\zeta_2}^3 + \lambda_1\zeta_1\right. \\ & \left. + l_{22}\mathrm{sign}\left(\zeta_2\right)\right) + \tfrac{1}{4}v_2^4 + \tfrac{3}{2}G_2^T G_2 v_2^2 \\ & - k_{p1}v_1^{4p} - k_{q1}v_1^{4q} - \tfrac{p_{\Theta 11}}{2\gamma_1}\tilde{\Theta}_1^{2p} \\ & - \tfrac{p_{\Theta 12}(2q-1)}{2q\gamma_1}\tilde{\Theta}_1^{2q} - \tfrac{1}{\gamma_2}\tilde{\Theta}_2\dot{\hat{\Theta}}_2 + \Xi_1.\end{aligned} \tag{45}$$

According to Lemma 4, one has

$$\frac{3}{2}G_2^T G_2 v_2^2 \leq \frac{3}{4}v_2^4\|G_2\|^4 + \frac{3}{4}. \tag{46}$$

Substituting (46) into (45) yields

$$\begin{aligned}\mathcal{L}V_2 \leq & v_2^3\left(u_x - \dot{\bar{\alpha}}_2 + \lambda_1\zeta_1 + l_{22}\mathrm{sign}\left(\zeta_2\right)\right. \\ & \left. + F_2\left(X_2\right)\right) + \tfrac{1}{4}v_2^4 + \tfrac{3}{4} \\ & - k_{p1}v_1^{4p} - k_{q1}v_1^{4q} - \tfrac{p_{\Theta 11}}{2\gamma_1}\tilde{\Theta}_1^{2p} \\ & - \tfrac{p_{\Theta 12}\,(2q-1)}{2q\gamma_1}\tilde{\Theta}_1^{2q} - \tfrac{1}{\gamma_2}\tilde{\Theta}_2\dot{\hat{\Theta}}_2 + \Xi_1,\end{aligned} \tag{47}$$

where $F_2\left(X_2\right) = 3v_2\|G_2\|^4/4 + l_{21}{\zeta_2}^3 + f_2$. The IT3FLS is introduced to approximate $F_2\left(X_2\right)$, i.e., $F_2\left(X_2\right) = \psi_2^T H_2\left(X_2\right) + \varepsilon_2\left(X_2\right)$. With Lemma 1, we assume that $|\varepsilon_2\left(X_2\right)| \leq \varepsilon_{2M}$, where $\varepsilon_{2M} \in R^+$.

Based on Lemma 4 again, we can obtain

$$\begin{aligned}v_2^3 F_2 \leq & \tfrac{1}{2a_{21}}v_2^6\Theta_2 H_2^T H_2 + \tfrac{3}{4a_{22}}v_2^4 \\ & + \tfrac{2a_{21} + a_{22}^3\varepsilon_{2M}^4}{4}, \\ v_2^3 l_{22}\mathrm{sign}\left(\zeta_1\right) \leq & \tfrac{3}{4a_{23}}v_2^4 + \tfrac{a_{23}^3}{4}l_{22}^4,\end{aligned} \tag{48}$$

where $a_{21}, a_{22}, a_{23} \in R^+$ are design constants, and $\Theta_2 = \max\|\psi_2\|^2$ is the learning parameter.

Substituting (48) into (47) yields

$$\begin{aligned}\mathcal{L}V_2 \leq & v_2^3\left(u_x - \dot{\bar{\alpha}}_2 + \lambda_1\zeta_1 + \tfrac{1}{2a_{21}}v_2^3\hat{\Theta}_2 H_2^T H_2\right. \\ & \left. + \tfrac{3}{4a_{22}}v_2 + \tfrac{1}{4}v_2\right) \\ & + \tfrac{3 + 2a_{21} + a_{22}^3\varepsilon_{2M}^4 + a_{23}^3 l_{22}^4}{4} \\ & - \tfrac{p_{\Theta 11}}{2\gamma_1}\tilde{\Theta}_1^{2p} - \tfrac{p_{\Theta 12}\,(2q-1)}{2q\gamma_1}\tilde{\Theta}_1^{2q} \\ & - \tilde{\Theta}_2\left(-\tfrac{1}{\gamma_2}\dot{\hat{\Theta}}_2 + \tfrac{1}{2a_{21}}v_2^6 H_2^T H_2\right) \\ & - k_{p1}v_1^{4p} - k_{q1}v_1^{4q} + \Xi_1.\end{aligned} \tag{49}$$

Design α_3 and $\hat{\Theta}_2$ for the second subsystem as follows:

$$\begin{aligned}\alpha_3 = & -k_{p2}v_2^{4p-3} - k_{q2}v_2^{4q-3} - \lambda_1\zeta_1 + \dot{\bar{\alpha}}_2 \\ & - \tfrac{1}{2a_{21}}v_2^6\hat{\Theta}_2 H_2^T H_2 - \tfrac{1}{4}v_2 - \tfrac{3}{4a_{22}}v_2 - \tfrac{3}{4a_{23}}v_2,\end{aligned} \tag{50}$$

$$\dot{\hat{\Theta}}_2 = -\frac{\gamma_2}{2a_{21}}v_2^6 H_2^T H_2 - p_{\Theta 21}\hat{\Theta}_2 - p_{\Theta 22}\hat{\Theta}_2^{2q-1}, \tag{51}$$

where $k_{p2}, k_{q2}, p_{\Theta 21}, p_{\Theta 22} \in R^+$ are design parameters.

Substituting (50) and (51) into (49) yields

$$\begin{aligned}\mathcal{L}V_2 \leq & -\sum_{i=1}^{2}k_{pi}v_i^{4p} - \sum_{i=1}^{2}k_{qi}v_i^{4q} - \tfrac{p_{\Theta 11}}{2\gamma_1}\tilde{\Theta}_1^{2p} \\ & - \tfrac{p_{\Theta 12}\,(2q-1)}{2q\gamma_1}\tilde{\Theta}_1^{2q} + \tfrac{p_{\Theta 21}}{\gamma_2}\tilde{\Theta}_2\hat{\Theta}_2 \\ & + \tfrac{p_{\Theta 22}}{\gamma_2}\tilde{\Theta}_2\hat{\Theta}_2^{2p-1} + v_2^3\left(u_x - \alpha_3\right) \\ & + \tfrac{3 + 2a_{21} + a_{22}^3\varepsilon_{2M}^4 + a_{23}^3 l_{22}^4}{4} + \Xi_1.\end{aligned} \tag{52}$$

It should be noted that

$$\begin{aligned}& \tfrac{p_{\Theta 21}}{\gamma_2}\tilde{\Theta}_2\hat{\Theta}_2 \leq \tfrac{p_{\Theta 21}}{2\gamma_2}\Theta_2^2 - \tfrac{p_{\Theta 21}}{2\gamma_2}\tilde{\Theta}_2^2, \\ & \left(\tilde{\Theta}_2^2\right)^p \leq \tilde{\Theta}_2^2 + (1-p)\,p^{\frac{p}{1-p}}, \\ & \tfrac{p_{\Theta 22}}{\gamma_2}\tilde{\Theta}_2\hat{\Theta}_2^{2q-1} \leq \tfrac{p_{\Theta 22}(2q-1)}{2q\gamma_2}\left(\Theta_2^{2q} - \tilde{\Theta}_2^{2q}\right).\end{aligned} \tag{53}$$

Substituting (53) into (52) yields

$$\begin{aligned}\mathcal{L}V_2 \leq & -\sum_{i=1}^{2}k_{pi}v_i^{4p} - \sum_{i=1}^{2}k_{qi}v_i^{4q} - \sum_{i=1}^{2}\tfrac{p_{\Theta i1}}{2\gamma_i}\tilde{\Theta}_i^{2p} \\ & - \sum_{i=1}^{2}\tfrac{p_{\Theta i2}(2q-1)}{2q\gamma_i}\tilde{\Theta}_i^{2q} + \sum_{i=1}^{2}\Xi_i + v_2^3\left(u_x - \alpha_3\right),\end{aligned} \tag{54}$$

where $\Xi_2 = p_{\Theta 21}\Theta_2^2/2\gamma_2 + (1-p)\,p_{\Theta 21}p^{p/(1-p)}/2\gamma_2 + \left(3 + 2a_{21} + a_{22}^3\varepsilon_{2M}^4 + a_{23}^3 l_{22}^4\right)/4 + (2q-1)\,p_{\Theta 22}\Theta_2^{2q}/2q\gamma_2$.

Steps 3 and 4: Given the similarity of these two steps to the derivations in Step 1 and Step 2, we will solely present the key expressions herein for space conservation.

Define the compensation signals ζ_3 and ζ_4 as follows:

$$\begin{aligned}\dot{\zeta}_3 = & -l_{31}{\zeta_3}^3 + \lambda_3\left(\bar{\alpha}_4 - \alpha_4\right) + \lambda_3\zeta_4 - \lambda_3 l_{32}\mathrm{sign}\left(\zeta_3\right), \\ \dot{\zeta}_4 = & -l_{41}{\zeta_4}^3 - \lambda_3\zeta_3 - l_{42}\mathrm{sign}\left(\zeta_4\right),\end{aligned} \tag{55}$$

where l_{31}, l_{32}, l_{41}, and l_{42} are design parameters.

From (5), (6), (9), (25)–(27), and (55), we can obtain

$$\begin{aligned}dv_3 = & \left(\lambda_3\left(v_4 + \alpha_4 + l_{32}\mathrm{sign}\left(\zeta_3\right) - \dot{x}_3^d\right.\right. \\ & \left.\left. - \tfrac{2}{\pi}\dot{\rho}_3\arctan\left(s_3\right)\right) + l_{31}{\zeta_3}^3\right)dt + G_3^T dw, \\ dv_4 = & \left(u_y + f_4 - \dot{\bar{\alpha}}_4 + l_{41}{\zeta_4}^3 + \lambda_3\zeta_3\right. \\ & \left. + l_{42}\mathrm{sign}\left(\zeta_4\right)\right)dt + G_4^T dw.\end{aligned} \tag{56}$$

Select the third and fourth Lyapunov function candidates as

$$\begin{aligned}V_3 = & V_2 + \tfrac{1}{4}v_3^4 + \tfrac{1}{2\gamma_3}\tilde{\Theta}_3^T\tilde{\Theta}_3, \\ V_4 = & V_3 + \tfrac{1}{4}v_4^4 + \tfrac{1}{2\gamma_4}\tilde{\Theta}_4^T\tilde{\Theta}_4,\end{aligned} \tag{57}$$

where $\tilde{\Theta}_3 = \Theta_3 - \hat{\Theta}_3$ and $\tilde{\Theta}_4 = \Theta_4 - \hat{\Theta}_4$ are estimation errors between ideal values Θ_3, Θ_4 and estimated values $\hat{\Theta}_3$, $\hat{\Theta}_4$, and γ_3, γ_4 are design parameters.

Let $F_3\left(X_3\right) = 3\lambda_3^3 v_3\|G_3\|^4/4 + l_{31}{\zeta_3}^3 v_3^3/\lambda_3$ and $F_4\left(X_4\right) = 3v_4\|G_4\|^4/4 + l_{41}{\zeta_4}^3 + f_4$. The IT3FLSs used to approximate these two nonlinear functions are $F_3\left(X_3\right) = \psi_3^T H_3\left(X_3\right) + \varepsilon_3\left(X_3\right)$ and $F_4\left(X_4\right) = \psi_4^T H_4\left(X_4\right) + \varepsilon_4\left(X_4\right)$, and we assume that $|\varepsilon_3| \leq \varepsilon_{3M}$ and $|\varepsilon_4\left(X_4\right)| \leq \varepsilon_{4M}$, where $\varepsilon_{3M} \in R^+$, $\varepsilon_{4M} \in R^+$. $\Theta_3 = \max\|\psi_3\|^2$ and $\Theta_4 = \max\|\psi_4\|^2$ are learning parameters.

Design α_4 and $\hat{\Theta}_3$ for the third subsystem as follows:

$$\begin{aligned}\alpha_4 = &-k_{p3}v_3^{4p-3} - k_{q3}v_3^{4q-3} - \tfrac{1}{2a_{31}}\lambda_3 v_3^3\hat{\Theta}_3 H_3^T H_3 \\ &- \tfrac{3}{4}\lambda_3^{\frac{1}{3}}v_3 - \tfrac{3}{4a_{32}}\lambda_3^{\frac{1}{3}}v_3 - \tfrac{3}{4a_{33}}\lambda_3^{\frac{1}{3}}v_3 \\ &+ \tfrac{2}{\pi}\dot{\rho}_3 \arctan(s_3) + \dot{x}_3^d,\end{aligned} \tag{58}$$

$$\dot{\hat{\Theta}}_3 = -\frac{\gamma_3}{2a_{31}}\lambda_3^2 v_3^6 H_3^T H_3 - p_{\Theta 31}\hat{\Theta}_3 - p_{\Theta 32}\hat{\Theta}_3^{2q-1}, \tag{59}$$

where $a_{31}, a_{32}, a_{33}, k_{p3}, k_{q3}, p_{\Theta 31}, p_{\Theta 32} \in R^+$ are design parameters.

Design α_5 and $\hat{\Theta}_4$ for the fourth subsystem as follows:

$$\begin{aligned}\alpha_5 = &-k_{p4}v_4^{4p-3} - k_{q4}v_4^{4q-3} + \dot{\bar{\alpha}}_4 - \lambda_3\zeta_3 \\ &- \tfrac{1}{2a_{41}}v_4^3\hat{\Theta}_4 H_4^T H_4 - \tfrac{1}{4}v_4 - \tfrac{3}{4a_{42}}v_4 - \tfrac{3}{4a_{43}}v_4,\end{aligned} \tag{60}$$

$$\dot{\hat{\Theta}}_4 = -\frac{\gamma_4}{2a_{41}}v_4^6 H_4^T H_4 - p_{\Theta 41}\hat{\Theta}_4 - p_{\Theta 42}\hat{\Theta}_4^{2q-1}, \tag{61}$$

where $a_{41}, a_{42}, a_{43}, k_{p4}, k_{q4}, p_{\Theta 41}, p_{\Theta 42} \in R^+$ are design parameters.

From (54), (57), and (56)–(59), we can obtain

$$\begin{aligned}\mathcal{L}V_4 \le &-\sum_{i=1}^{4} k_{pi}v_i^{4p} - \sum_{i=1}^{4} k_{qi}v_i^{4q} + \sum_{i=1}^{4}\Xi_i - \sum_{i=1}^{4}\tfrac{p_{\Theta i1}}{2\gamma_i}\tilde{\Theta}_i^{2p} \\ &- \sum_{i=1}^{4}\tfrac{p_{\Theta i2}(2q-1)}{2q\gamma_i}\tilde{\Theta}_i^{2q} + v_2^3(u_x - \alpha_3) + v_4^3(u_y - \alpha_5),\end{aligned} \tag{62}$$

where $\Xi_3 = p_{\Theta 31}\Theta_3^2/2\gamma_3 + (1-p)p_{\Theta 31}p^{p/(1-p)}/2\gamma_3 + \left(3 + 2a_{31} + a_{32}^3\varepsilon_{3M}^4 + a_{33}^3 l_{32}^4\right)/4 + (2q-1)p_{\Theta 32}\Theta_3^{2q}/2q\gamma_3$ and $\Xi_4 = p_{\Theta 41}\Theta_4^2/2\gamma_4 + (1-p)p_{\Theta 41}p^{p/(1-p)}/2\gamma_4 + \left(3 + 2a_{41} + a_{42}^3\varepsilon_{4M}^4 + a_{43}^3 l_{42}^4\right)/4 + (2q-1)p_{\Theta 42}\Theta_4^{2q}/2q\gamma_4$.

Step 5: The STETM is introduced in this step for data transmission. For simplicity, let $v_x = v_2$, $v_y = v_4$, $\alpha_x = \alpha_3$, $\alpha_y = \alpha_4$. Then, the intermediate control signals are designed as follows: $(i = x, y)$

$$\omega_i = -(1+\aleph_i)\left[\alpha_i \tanh\left(\frac{v_i^3\alpha_i}{\wp_i}\right) + \bar{m}_i \tanh\left(\frac{v_i^3\bar{m}_i}{\wp_i}\right)\right]. \tag{63}$$

Define the corresponding trigger mechanism as follows:

$$\begin{aligned}&u_i = \omega_i\left(t_i^k\right), \forall t_i \in \left[t_i^k, t_i^{k+1}\right), \delta_i = \omega_i - u_i, \\ &t_i^{k+1} = \begin{cases} \inf\left\{t_i > t_i^k \,||\delta_i| \ge n_i\right\}, |u_i| \ge D_i, \\ \inf\left\{t_i > t_i^k \,||\delta_i| \ge \aleph_i|u_i| + m_i\right\}, |u_i| < D_i, \end{cases}\end{aligned} \tag{64}$$

where D_i, $\aleph_i$, n_i, m_i, $\bar{m}_i$, and $\wp_i$ denote design parameters, and $\delta_i, i = x, y$ denote the measurement errors. Term t_i^k are the update times of the controller, while $0 < \aleph_i < 1$ and $\bar{m}_i > m_i/(1-\aleph_i)$. The control signals hold as $u_i\left(t_i^k\right)$ during the time $\left[t_i^k, t_i^{k+1}\right]$. When the ETM is triggered, the time will be set instantly as t_i^{k+1}. Then, the control signals $u_i\left(t_i^{k+1}\right)$ will be applied.

Remark 8: As observed from the trigger mechanism (64), the introduced STETM incorporates a combined approach of fixed and relative threshold design methods. More specifically, when the control input signals satisfy $|u_i| < D_i$, the control system adopts a relative threshold strategy to achieve precise control. Conversely, when $|u_i|$ exceed a certain value, the relative threshold policy is switched to a fixed threshold policy, ensuring that the measurement errors δ_i remain within bounds to maintain a certain level of system performance. This threshold design scheme combines the benefits of both fixed threshold and relative threshold design strategies, offering enhanced flexibility and allowing the system to make appropriate adjustments in order to save communication resources while balancing system performance.

Remark 9: Unlike finite-time control schemes [17]–[22], [29], [39], where the stability time depends on the initial state of the system, in this paper, the controller is designed based on the fixed-time stability theory [22]. Therefore, the proposed control scheme ensures that the settling time is completely determined by the design parameters.

B. Stability Analysis

Theorem 1: For the stochastic MEMS gyroscope (5) under Assumptions 1, the virtual control signals (37), (50), (58), (60), the adaptive laws (38), (51), (59), (61), the intermediate control signal (63), and the switching threshold event-triggered rules (64), all the closed-loop system signals are FTBIP and the tracking errors are within the prescribed performance boundaries within a fixed time.

Proof: From (64), one has

$$\omega_i = (1 + \hbar_{i1}\aleph_i)u_i + \hbar_{i2}m_i, \tag{65}$$

where $\hbar_{i1}$ and $\hbar_{i2}$ are continuous time-varying parameters with $\hbar_{i1}(0) = \hbar_{i2}(0) = 0$ and $|\hbar_{i1}|, |\hbar_{i2}| \le 1$. It should be noted that

$$\frac{v_i\omega_i}{1+\hbar_{i1}\aleph_i} \le \frac{v_i\omega_i}{1+\aleph_i}, \left|\frac{\hbar_{i2}m_i}{1+\hbar_{i1}\aleph_i}\right| \le \frac{m_i}{1-\aleph_i} < \bar{m}_i. \tag{66}$$

With Lemma 5 and (66), one can obtain

$$\begin{aligned}&v_i^3(u_i - \alpha_i) \\ &= -v_i^3\left[\alpha_i \tanh\left(\tfrac{v_i^3\alpha_i}{\wp_i}\right) + \bar{m}_i \tanh\left(\tfrac{v_i^3\bar{m}_i}{\wp_i}\right) - \alpha_i - \bar{m}_i\right] \\ &\le \left|v_i^3\alpha_i\right| - v_i^3\alpha_i \tanh\left(\tfrac{v_i^3\alpha_i}{\wp_i}\right) + \left|v_i^3\bar{m}_i\right| \\ &-v_i^3\bar{m}_i \tanh\left(\tfrac{v_i^3\bar{m}_i}{\wp_i}\right) \le 0.557\wp_i.\end{aligned} \tag{67}$$

Select the Lyapunov function as follows:

$$V = \sum_{i=1}^{4}\frac{1}{4}v_i^4 + \sum_{i=1}^{4}\frac{1}{2\gamma_i}\tilde{\Theta}_i^T\tilde{\Theta}_i. \tag{68}$$

Combining (62) , (67) and (68) yields

$$\begin{aligned}\mathcal{L}V \le &-\sum_{i=1}^{4} k_{pi}v_i^{4p} - \sum_{i=1}^{4} k_{qi}v_i^{4q} - \sum_{i=1}^{4}\tfrac{p_{\Theta i1}}{2\gamma_i}\tilde{\Theta}_i^{2p} \\ &- \sum_{i=1}^{4}\tfrac{p_{\Theta i2}(2q-1)}{2q\gamma_i}\tilde{\Theta}_i^{2q} + \sum_{i=1}^{4}\Xi_i + 0.557(\wp_x + \wp_y).\end{aligned} \tag{69}$$

From (69), one has

$$\begin{aligned}\mathcal{L}V \le &-\sigma_1\left(\sum_{i=1}^{4} v_i^{4p} + \sum_{i=1}^{4}\tilde{\Theta}_i^{2p}\right) \\ &-\sigma_2\left(\sum_{i=1}^{4} v_i^{4q} + \sum_{i=1}^{4}\tilde{\Theta}_i^{2q}\right) + \beta\end{aligned} \tag{70}$$

where $\sigma_1 = \min\{4k_{pi}, p_{\Theta i1}\}$, $\sigma_2 = \min\left\{4k_{qi}, \frac{(2q-1)p_{\Theta i1}}{q}\right\}$, $\beta = \sum_{i=1}^{4}\Xi_i + 0.557(\wp_x + \wp_y)$. By selecting suitable constants σ_1, σ_2 and β, Lemma 2 allows us to conclude that both

the states v_i and the parameter estimation errors $\tilde{\Theta}_i$ are all FTBIP. Furthermore, given the introduction of ECM into the system, it becomes imperative to confirm that $\zeta_i, i = 1, 2, 3, 4$ are FTBIP.

Select the Lyapunov function as follows:

$$V_\zeta = \sum_{i=1}^{4} \frac{1}{2}\zeta_i^2. \tag{71}$$

Calculating its time derivative yields

$$\begin{aligned} dV_\zeta = & -l_{11}{\zeta_1}^4 + \lambda_1\zeta_1\left(\bar{\alpha}_2 - \alpha_2\right) + \lambda_1\zeta_1\zeta_2 - \lambda_1 l_{12}\left|\zeta_1\right| \\ & - l_{31}{\zeta_3}^4 + \lambda_3\zeta_3\left(\bar{\alpha}_4 - \alpha_4\right) + \lambda_3\zeta_3\zeta_4 - \lambda_3 l_{32}\left|\zeta_3\right| \\ & - l_{21}{\zeta_2}^4 - \lambda_1\zeta_1\zeta_2 - l_{22}\left|\zeta_2\right| - l_{41}{\zeta_4}^4 \\ & - \lambda_3\zeta_3\zeta_4 - l_{42}\left|\zeta_4\right| \\ = & -\sum_{i=1}^{4} l_{i1}{\zeta_i}^4 + \sum_{i=1,3} \lambda_i\zeta_i\left(\bar{\alpha}_i - \alpha_i\right) - \sum_{i=1}^{4} \Delta_i l_{i2}\left|\zeta_i\right| \end{aligned} \tag{72}$$

where $\Delta_i = \lambda_i, i = 1, 3$ and $\Delta_i = 1, i = 2, 4$. According to Lemmas 3 and 6, one has $\bar{\alpha}_i - \alpha_i \leq \eta_i$ within a fixed time T_{iF}. Then, we can obtain

$$\begin{aligned} dV_\zeta \leq & -\sum_{i=1}^{4} l_{i1}{\zeta_i}^4 - \sum_{i=1,3} \Delta_i\left(l_{i2} - \eta_{i+1}\right)\left|\zeta_i\right| - \sum_{i=2,4} l_{i2}\left|\zeta_i\right| \\ \leq & -\iota_1 V_\zeta^{\frac{1}{2}} - \iota_2 V_\zeta^2, \end{aligned} \tag{73}$$

where $\iota_1 = \sqrt{2}\min\left\{\lambda_1\left(l_{12} - \eta_2\right), \lambda_3\left(l_{32} - \eta_4\right), l_{22}, l_{42}\right\}$, and $\iota_1 = \min\left\{l_{11}, l_{21}, l_{31}, l_{41}\right\}$.

From (73) and Lemma 2, we know ζ_i are FIBIP with the settling time $T_\zeta = 2/\iota_1 + 1/\iota_2$. Moreover, since $z_i = v_i + \zeta_i$, then z_i are FIBIP. From (6), (25), and Assumptions 1, we can determine that $s_i, i = 1, 3$ and $x_i, i = 2, 4$ are FIBIP. Besides, it can be observed from (8) that the boundedness of s_i means that $-1 < e_i/\rho_i < 1$. In other words, $e_i \in \Omega_{e_i}, i = 1, 3$ always hold. Therefore, the prescribed performance boundaries of tracking errors with a fixed time can be guaranteed. Moreover, from Lemmas 2 and 3, we can deduce that the settling time satisfies $T = 1/\left[\sigma_1(1-p)\right] + 1/\left[\sigma_2(q-1)\right] + \sum_{i=1}^{4} T_{iF} + T_\zeta$.

Next, it should be noted that $\delta_i = \omega_i - u_i$ for $\forall t_i \in \left[t_i^k, t_i^{k+1}\right)$. Hence, one obtains

$$\frac{d}{dt}\left|\delta_i\right| \leq \frac{d}{dt}\left(\delta_i \times \delta_i\right)^{\frac{1}{2}} = \operatorname{sign}\left(\delta_i\right)\dot{\delta}_i \leq \left|\dot{\omega}_i\right|. \tag{74}$$

Since $\dot{\omega}_i$, $i = x, y$ are bounded, $\dot{\omega}_i$ continuously connect to the bounded signals when $t_i \in \left[t_i^k, t_i^{k+1}\right)$. In other words, there exists positive constants Υ_i such that $\left|\dot{\omega}_i\right| \leq \Upsilon_i$, $t_i \in \left[t_i^k, t_i^{k+1}\right)$, $i = x, y$, leading to the conclusion that $\left|\delta_i\right| \leq \Upsilon_i\left(t_i - t_i^{k+1}\right)$, $t_i \in \left[t_i^k, t_i^{k+1}\right)$. It should be noted that $\delta_i\left(t_i^k\right) = 0$ and $\lim_{t_i \to t_i^{k+1}} \left|\delta_i\right| \leq \aleph_i\left|\omega_i\left(t_i^{k+1}\right)\right| + m_i$; thus, one has

$$m_i \leq \lim_{t_i \to t_i^{k+1}} \left|\delta_i\right| \leq \Upsilon_i \Delta t_i, \tag{75}$$

where $\Delta t_i = t_i^{k+1} - t_i^k$. Evidently, $\Delta t_i > 0$ can be easily deduced for any finite time interval. Additionally, $t_i^k \to \infty$ can be observed as $k \to \infty$, which can be verified by contradiction. Specifically, assuming $t_i^\infty = \lim_{k\to\infty} t_i^k < \infty$ implies that $\lim_{k\to\infty} \Delta t_i = 0$. In conjunction with eq (75), it results that $0 < m_i \leq \Upsilon_i \times 0 = 0$, $k \to \infty$. Having considered the preceding discussion, we can assert that the occurrence of Zeno behavior can be effectively eliminated. Up to now, we have completed the proof of Theorem 1.

Remark 10: A discussion on the effect of the control parameters is detailed below.

1) By increasing the control gains k_{pi}, k_{qi}, $i = 1, 2, 3, 4$, the adaptive gains $p_{\Theta i1}$, $p_{\Theta i2}$, the filter gains l_{i1}, and decreasing the filter gains l_{i2}, the upper bound of v_i can be reduced to achieve a more effective tracking. However, excessively large values of $k_{pi}, k_{qi}, p_{\Theta i1}, p_{\Theta i2}, l_{i1}$ and excessively small values of l_{i2} can lead to surges and vibrations in control inputs, potentially causing damage to the control system. Therefore, it is important to moderately adjust these control parameters to ensure satisfactory tracking performance without exceeding the control system's input capability.
2) The parameters of the QPPF (7) need to be adjusted according to the actual application requirements. Specifically, parameters ρ_{i0}, $i = 1, 3$ should encompass the initial position of the system states $x_i(0)$, while parameters $\rho_{i\infty}$ must be fine-tuned based on the specific application needs. Theoretically, the values of $\rho_{i\infty}$ can approach infinitesimal levels. However, as $\rho_{i\infty}$ decrease, the control signals amplify, leading to higher energy consumption. Therefore, in practical engineering applications, a trade-off between the control signals and the steady-state limit boundary must be maintained. Additionally, increasing parameters ℓ_i can improve error convergence speed, but excessively large values of ℓ_i may introduce overshoots and vibrations. Hence, selecting moderate values for ℓ_i, tailored to the specific application requirements, is crucial.
3) The performance of the filter (26) can be improved by decreasing the filter parameters r_{i1}, h_{i1}, $i = 2, 4$, and increasing r_{i2}, h_{i2}, M, N. However, pursuing an extreme filtering performance may lead to unbounded growth in control inputs. Therefore, it is essential to maintain a balance between filtering performance and control inputs when adjusting the filtering parameters.
4) The performance of STETM (63) and (64) can be enhanced by decreasing parameters $\aleph_i, \wp_i$, $i = x, y$. Nevertheless, excessively small values of $\aleph_i, \wp_i$ may lead to an increased frequency of trigger occurrences. Therefore, it is important to avoid setting $\aleph_i, \wp_i$ too small. Additionally, parameters $n_i, m_i, \bar{m}_i$ influence the trigger threshold. Specifically, larger values of $n_i, m_i, \bar{m}_i$ may delay event triggering, whereas smaller values of $n_i, m_i, \bar{m}_i$ may lead to more frequent event triggering. The adjustment of parameters D_i has been detailed in Remark 8.
5) The remaining control parameters, such as a_{i1}, a_{i2}, a_{i3}, $i = 1, 2, 3, 4$ are utilized to address potential singularity issues that may arise from the introduction of inequality transformations. In cases where such singularity problems occur, these parameters can be decreased to prevent singularity and ensure the controller's normal

operation. Parameter γ_i serves a similar purpose, yet it is distinctively used to mitigate singularity issues when employing fuzzy approximators.

IV. SIMULATION RESULTS

This section presents the numerical experiments that were conducted to verify the feasibility and effectiveness of the proposed control scheme for the MEMS gyroscope. The system parameters were selected as follows [3]: $m = 1.8 \times 10^{-7}\text{kg}$, $\Omega_z^* = 100\text{rad/s}$, $\omega_0 = 1000\text{HZ}$, $d_{xx}^* = 1.8 \times 10^{-6}\text{Ns/m}$, $d_{yy}^* = 3.6 \times 10^{-7}\text{Ns/m}$, $d_{xy}^* = 1.8 \times 10^{-6}\text{Ns/m}$, $k_{xx}^* = 63.955\text{N/m}$, $k_{yy}^* = 95.92\text{N/m}$, and $k_{xy}^* = 12.799\text{N/m}$, and the desired tracking signals were set as $x_1^d = 1.36\sin(2t) + 0.14$ and $x_3^d = 1.32\sin(t) + 0.18$.

Simulation 1: (Effectiveness and superiority of the proposed controller):

Case 1: The main control parameters were chosen as $k_{p1} = k_{p3} = 75$, $k_{p2} = k_{p4} = 30$, $k_{q1} = k_{q3} = 75$, $k_{q2} = k_{q4} = 30$, $l_{11} = l_{21} = l_{31} = l_{41} = 20$, $l_{12} = l_{22} = l_{32} = l_{42} = 0.01$, $a_{11} = a_{21} = a_{31} = a_{41} = 0.75$, $a_{12} = a_{22} = a_{32} = a_{42} = 0.1$, $a_{13} = a_{23} = a_{33} = a_{43} = 0.5$, $r_{21} = r_{41} = 1$, $r_{22} = r_{42} = 20$, $h_{21} = h_{41} = 1$, $h_{22} = h_{42} = 20$, $\mu_{21} = \mu_{22} = \mu_{41} = \mu_{42} = 1$, $M = N = 20$, $\gamma_1 = \gamma_1 = \gamma_1 = \gamma_1 = 0.2$, $p_{\Theta 11} = p_{\Theta 21} = p_{\Theta 31} = p_{\Theta 41} = 10$, $p_{\Theta 12} = p_{\Theta 22} = p_{\Theta 32} = p_{\Theta 42} = 10$, $\ell_1 = \ell_3 = 1$, $\rho_{10} = 0.6$, $\rho_{30} = 0.5$, and $\rho_{1\infty} = \rho_{3\infty} = 0.1$. For IT3FLS, consider five membership functions centered on $-1, -0.25, 0, 0.75$, and 1, and five rules. The initial conditions were $x_1(0) = 0.2$, $x_3(0) = 0.15$, $x_2(0) = x_4(0) = 0$, $\hat{\Theta}_1(0) = \hat{\Theta}_3(0) = 0.01$, $\hat{\Theta}_2(0) = \hat{\Theta}_4(0) = 0$, $\varphi_{21}(0) = \varphi_{22}(0) = 0$, $\varphi_{41}(0) = \varphi_{42}(0) = 0$, $\bar{\alpha}_2(0) = \alpha_2(0) = 0$, and $\bar{\alpha}_4(0) = \alpha_4(0) = 0$.

Case 2: Based on Case 1, the unknown variations of spring and damping terms were further considered as
$\Delta d_{xx}^* = 0.4 \times d_{xx}^* \times \text{sign}(x), \Delta d_{yy}^* = 0.35 \times d_{yy}^* \times \text{sign}(y),$
$\Delta d_{xy}^* = 0.3 \times d_{xy}^* \times \text{sign}(x) + 0.3 \times d_{xy}^* \times \text{sign}(y),$
$\Delta k_{xx}^* = 0.3 \times k_{xx}^* \times \text{sign}(x), \Delta k_{yy}^* = 0.35 \times k_{yy}^* \times \text{sign}(y),$
$\Delta k_{xy}^* = 0.3 \times k_{xy}^* \times \text{sign}(x) + 0.3 \times k_{xy}^* \times \text{sign}(y).$
Additionally, the stochastic disturbances were chosen as
$G_1 = (1 - \cos(x_1\pi/180)) \times \text{randn},$
$G_2 = (1 - \sin(x_2\pi/180)) \times \text{randn},$
$G_3 = (x_3 \sin(x_2\pi/180)) \times \text{randn},$
$G_4 = (x_4 \sin(x_3\pi/180)) \times \text{randn},$
where randn represents a random number that conforms to a normal distribution.

Case 3 and Case 4: To demonstrate the potential advantages of the control scheme proposed in this paper, the control results of the controllers in literature [48] (Case 3) and literature [49] (Case 4) were presented for the stochastic MEMS gyroscope. The system parameters were set according to Case 1, while the applied stochastic disturbances were based on Case 2.

Case 5: Based on Case 2, to showcase the superior handling of stochastic disturbances by the IT3FLS, we compared and evaluated the tracking performance of controllers based on the radial basis function (RBF), type-1 fuzzy logic system (T1FLS), type-2 fuzzy logic system (T2FLS), and IT3FLS.

Case 6: Based on Case 2, to directly analyze the computational burden of the IT3FLS, we compared the execution time between different fuzzy-based methods. The simulations were conducted using Matlab 2019b on a system with an Intel® Core™ i7-8700 CPU @ 3.20GHz and 8GB of RAM.

TABLE II
COMPARATIVE RESULTS OF TRACKING PERFORMANCE INDICES

Indices	Case 1	Case 2	Case 3	Case 4
μ_{e_1}	0.0013	0.0014	0.0068	0.0064
μ_{e_3}	0.0008	0.0010	0.0095	0.0094
S_{e_1}	0.0053	0.0056	0.0150	0.0159
S_{e_2}	0.0027	0.0027	0.0162	0.0153

TABLE III
COMPARISON OF PROPOSED CONTROLLER WITH VARIOUS NEURO-FUZZY SYSTEMS

Indices	RBF	T1FLS	T2FLS	IT3FLS
μ_{e_1}	0.0031	0.0031	0.0020	0.0014
μ_{e_3}	0.0026	0.0027	0.0017	0.0010
S_{e_1}	0.0122	0.0125	0.0095	0.0053
S_{e_2}	0.0094	0.0089	0.0067	0.0027

Simulation 2: (Superiority of QPPF):

Case 1: Based on Simulation 1 (Case 2), resetting $\ell_1 = \ell_3 = 2$, and comparing the QPPF with the TPPF.

Case 2: Based on Simulation 1 (Case 2), resetting $\ell_1 = \ell_3 = 5$, and comparing the QPPF with the TPPF.

Simulation 3: (Superiority of ETM):

Based on Simulation 1 (Case 2), the event-triggered parameters were selected as follows: $D_x = D_y = 125$, $\aleph_x = \aleph_y = 0.1$, $\wp_x = \wp_y = 0.1$, $\bar{m}_x = \bar{m}_y = 10$, $n_x = n_y = 10$, $m_x = m_y = 10$.

In this paper, the following four performance indices are used to quantitatively analyze the control effectiveness:

$$\mu_{e_i} = \frac{1}{N}\sum_{j=1}^{N}|e_i(j)| \tag{76}$$

$$S_{e_i} = \sqrt{\frac{1}{N}\sum_{j=1}^{N}[|e_i(j) - \mu_{e_i}|]} \tag{77}$$

$$\begin{aligned} M_{u_m} = & \max_{j=1,\ldots,N}\{[u_m(j) - \mu_{u_m}]\} \\ & - \min_{j=1,\ldots,N}\{[u_m(j) - \mu_{u_m}]\} \end{aligned} \tag{78}$$

$$F_{c_m} = \frac{M_{u_m}}{\frac{1}{N}\sum\limits_{j=1}^{N}u_m(j)} \tag{79}$$

where $\mu_{e_i}$and S_{e_i} are the mean and standard deviation of $e_i, i = 1, 3$, respectively, $M_{u_m}$and F_{c_m} are are the amplitude and vibration factor values of $u_m, m = x, y$, respectively, and N denotes the number of sample points.

The MATLAB was utilized to obtain the simulation results presented in Figs 3–5. A fixed step size of 0.001 was employed throughout the simulations.

Fig. 3 illustrates the trajectory tracking and tracking errors between the actual and the reference trajectory of the MEMS gyroscope. As demonstrated in Fig. 3, despite the existence of stochastic disturbances and unknown variations, the actual

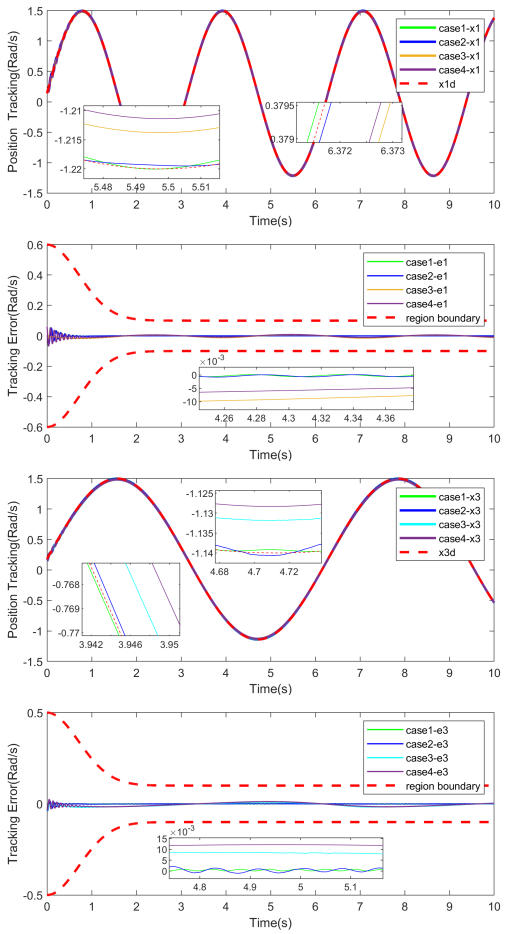

Fig. 3. Tracking results of x_1 and x_3.

TABLE IV
COMPARISON OF EXECUTION TIMES

Indices	T1FLS	T2FLS	IT3FLS
Execution time (s)	36.329657	37.400013	39.213035

trajectory closely approximated the reference trajectory with minimal errors and remained within the specified bound. Table II provides the relevant tracking performance indices. Comparing the control performance of the MEMS gyroscope with and without unknown variations and stochastic disturbances, it is evident that these factors scarcely affected the control performance of the controller under the QPPF constraints. Moreover, the proposed scheme demonstrated both lower tracking errors (smaller mean and standard deviation values) for the MEMS gyroscope compared to the methods presented in [48] and [49].

Additionally, based on Table III, it is evident that the IT3FLS exhibited a considerable enhancement in tracking accuracy when compared to conventional neural-fuzzy systems. This result highlights the superior capability of the IT3FLS in effectively handling stochastic disturbances.

Furthermore, Table IV validates that the execution time of the IT3FLS was marginally longer compared to conventional FLS-based methods. However, it's worth mentioning

TABLE V
COMPARATIVE RESULTS OF CONTROL INPUT CHATTERING

Indices	Case1-QPPF	Case1-TPPF	Case2-QPPF	Case2-TPPF
M_{u_x}	371.6798	388.1492	374.2849	417.4556
M_{u_y}	201.4831	208.8479	201.8316	220.4914
F_{c_x}	17.7243	18.5097	17.8577	19.9203
F_{c_y}	5.0721	5.2557	5.0803	5.5491

that besides CPU performance, the programming approach employed in FLSs also influences the execution time. Utilizing vector programming and minimizing loops can significantly enhance time efficiency. Moreover, with the progress of high-speed programmable ICs, the slightly longer execution time of the IT3FLS does not lead to a substantial increase in computational burden.

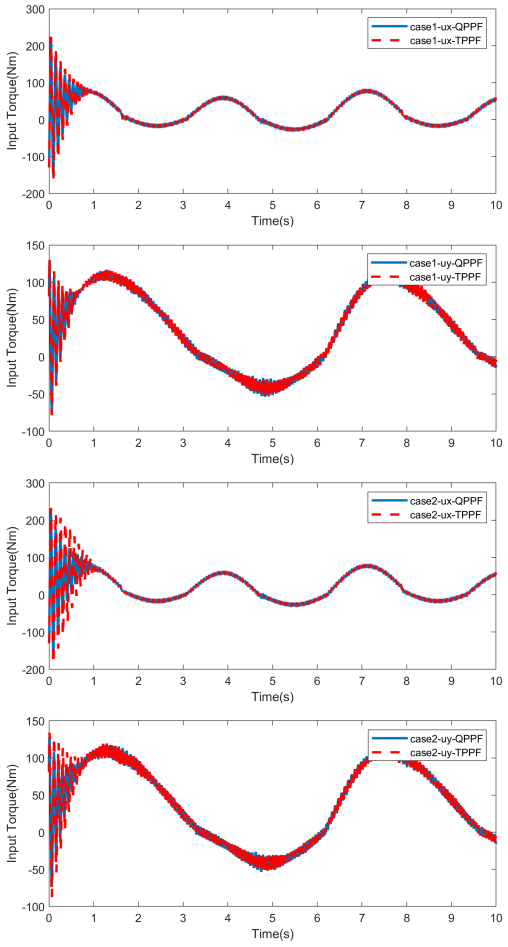

Fig. 4. Vibration evaluation results of u_x and u_y.

Fig. 4 showcases a comparison of the control input torques provided by the QPPF and the TPPF for different values of ℓ_i, from which it is evident that the control inputs of the QPPF and the TPPF were essentially similar at smaller values of ℓ_i. However, as ℓ_i became sufficiently large, the TPPF exhibited more pronounced vibrations during the initial stage of control input compared to the QPPF (note that the area covered in red is larger in the initial phase). Corresponding comparative index values are presented in Table V, which demonstrates

TABLE VI
COMPARISON BETWEEN EMT AND CCT

Indices	Relative	Switching	Fixed	Continuous-time
u_x	142	210	337	10000
u_y	63	150	225	10000
μ_{e_1}	0.0016	0.0016	0.0015	0.0014
μ_{e_3}	0.0012	0.0010	0.0010	0.0010
S_{e_1}	0.0065	0.0058	0.0057	0.0053
S_{e_3}	0.0035	0.0034	0.0031	0.0027

that the proposed QPPF effectively mitigated the initial control vibrations for the MEMS gyroscope.

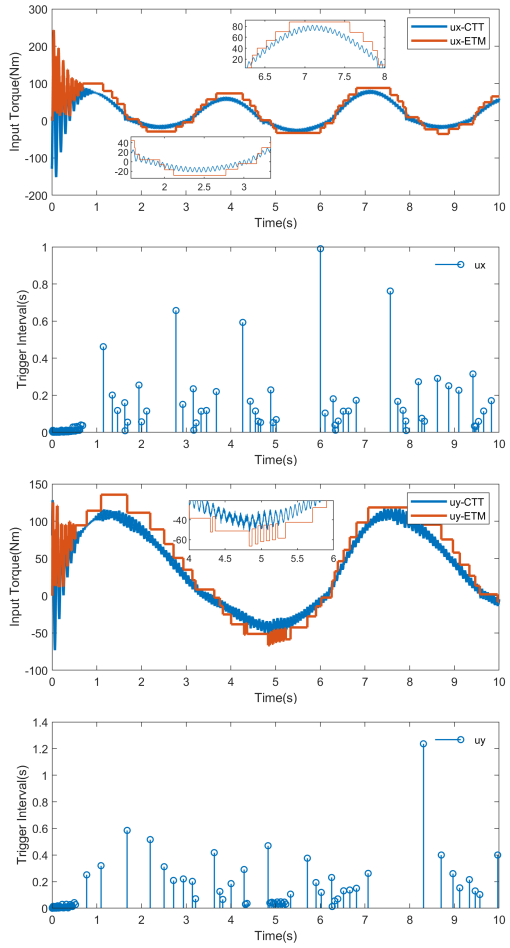

Fig. 5. Event-triggered results of u_x and u_y.

Fig. 5 provides valuable insights into the control input and switching threshold event-triggered frequency of the MEMS gyroscope. The results depicted in Fig. 5 and summarized in Table VI demonstrate that the control scheme utilizing the STETM is effective in reducing the reliance on frequent communication while preserving control accuracy, as compared to the control scheme employing the continuous-time-triggered mechanism. Furthermore, the STETM strikes a balance between triggered times and tracking accuracy, in contrast to control schemes based on relative thresholds and fixed threshold event-triggered mechanisms. Additionally, Fig. 5 reveals that during the initial phase, the controller required frequent triggers to track the reference signal rapidly. However, as the process progressed, the system reached a relatively stable state, significantly increasing the average time interval between trigger events. Furthermore, the control input based on the STETM exhibited a vibration-shielding effect. These findings underline the significance of implementing the STETM in MEMS gyroscope control applications.

V. CONCLUSION

This article effectively addressed the challenge of developing fixed-time fuzzy vibration reduction control for stochastic MEMS gyroscopes. The combination of the CFBBD with the ECM in the proposed approach was aimed at addressing the issue of complexity explosion and compensating for filtering errors. Moreover, the QPPF was designed to drive the tracking error towards a small neighborhood of zero within a predefined period and reduce control vibrations. The employment of the STETM ensured efficient resource utilization and vibration filtration without sacrificing control accuracy. The simulation results substantiated the effectiveness and superiority of the proposed control strategy in attaining the desired control performance of MEMS gyroscopes.

REFERENCES

[1] M. Solouk, M. Shojaeefard, and M. Dahmardeh, "Parametric topology optimization of a MEMS gyroscope for automotive applications," *Mech. Syst. Signal Process.*, vol. 128, pp. 389-404, Aug. 2019.

[2] X. Shao, H. Si, and W. Zhang, "Low-frequency learning quantized control for MEMS gyroscopes accounting for full-state constraints," *Eng. Appl. Artif. Intell.*, vol. 115, no. 104724, Oct. 2022.

[3] X. Shao and Y. Shi, "Neural-Network-Based Constrained Output-Feedback Control for MEMS Gyroscopes Considering Scarce Transmission Bandwidth," *IEEE Trans. Cybern.*, vol. 52, no. 11, pp. 12351-12363, Nov. 2022.

[4] H. Zhang and F. Chen, "Observer-based prescribed performance tracking control for MEMS Gyroscope subject to input saturation," *Nonlinear Dyn.*, vol. 110, no. 4, pp. 3395-3410, Dec. 2022.

[5] X. Shao and Y. Shi, "Neural Adaptive Control for MEMS Gyroscope With Full-State Constraints and Quantized Input," *IEEE Trans. Ind. Inform.*, vol. 16, no. 10, pp. 6444-6454, Oct. 2020.

[6] J. Fei and J. Zhou, "Robust Adaptive Control of MEMS Triaxial Gyroscope Using Fuzzy Compensator," *IEEE Trans. Syst. Man Cybern. Part B-Cybern.*, vol. 42, no. 6, pp. 1599-1607, Dec. 2012.

[7] W. Juan and J. Fei, "Adaptive fuzzy approach for non-linearity compensation in MEMS gyroscope," *Trans. Inst. Meas. Control*, vol. 35 no. 8, pp. 1008-1015, Dec. 2013.

[8] S. Luo, G. Yang, J. Li, and H. Ouakad, "Dynamic analysis, circuit realization and accelerated adaptive backstepping control of the FO MEMS gyroscope," *Chaos Solitons Fractals*, vol. 155, no. 111735, Feb. 2022.

[9] F. Li, S. Luo, S. He, and H. Ouakad, "Dynamical analysis and accelerated adaptive backstepping control of MEMS triaxial gyroscope with output constraints," *Nonlinear Dyn.*, vol. 111, no. 18, pp. 17123-17140, Sep. 2023.

[10] J. Rickard, J. Aisbett and G. Gibbon, "Fuzzy Subsethood for Fuzzy Sets of Type-2 and Generalized Type- n," *IEEE Trans. Fuzzy Syst.*, vol. 17, no. 1, pp. 50-60, Feb. 2009.

[11] A. Mohammadzadeh, M. Sabzalian and W. Zhang, "An Interval Type-3 Fuzzy System and a New Online Fractional-Order Learning Algorithm: Theory and Practice," *IEEE Trans. Fuzzy Syst.*, vol. 28, no. 9, pp. 1940-1950, Sep. 2020.

[12] P. Ochoa, O. Castillo, P. Melin, and J. Castro, "Interval type-3 fuzzy differential evolution for parameterization of fuzzy controllers," *Int. J. Fuzzy Syst.*, vol. 25, no. 4, pp. 1360-1376, Jun. 2023.

[13] L. Amador-Angulo, O. Castillo, J. Castro, and P. Melin, "A new approach for interval type-3 fuzzy control of nonlinear plants," *Int. J. Fuzzy Syst.*, vol. 25, no. 4, pp. 1624-1642, Jun. 2023.

[14] C. Peraza, O. Castillo, P. Melin, J. Castro, J. Yoon, and Z. Geem, "A type-3 fuzzy parameter adjustment in harmony search for the parameterization of fuzzy controllers," *Int. J. Fuzzy Syst*., doi: 10.1007/s40815-023-01499-w.

[15] O. Castillo, J. Castro, and P. Melin, "Interval type-3 fuzzy control for automated tuning of image quality in televisions," *Axioms*, vol. 11 no. 6, no. 276, Jun. 2022.

[16] O. Castillo, J. Castro, P. Melin, "A methodology for building interval type-3 fuzzy systems based on the principle of justifiable granularity," *Int. J. Fuzzy Syst*., vol. 37, no. 10, pp. 7909-7943, Oct. 2022.

[17] S. Bhat and D. Bernstein, "Continuous finite-time stabilization of the translational and rotational double integrators," *IEEE Trans. Autom. Control*, vol. 43, no. 5, pp. 678-682, May. 1998.

[18] S. Sui, C. Chen and S. Tong, "Event-Trigger-Based Finite-Time Fuzzy Adaptive Control for Stochastic Nonlinear System With Unmodeled Dynamics," *IEEE Trans. Fuzzy Syst*., vol. 29, no. 7, pp. 1914-1926, Jul. 2021.

[19] S. Sui, C. Chen and S. Tong, "Finite-Time Adaptive Fuzzy Prescribed Performance Control for High-Order Stochastic Nonlinear Systems," *IEEE Trans. Fuzzy Syst*., vol. 30, no. 7, pp. 2227-2240, Jul. 2022.

[20] J. Xia, B. Li, S. Su, W. Sun and H. Shen, "Finite-Time Command Filtered Event-Triggered Adaptive Fuzzy Tracking Control for Stochastic Nonlinear Systems," *IEEE Trans. Fuzzy Syst*., vol. 29, no. 7, pp. 1815-1825, Jul. 2021.

[21] H. Min, S. Xu and Z. Zhang, "Adaptive Finite-Time Stabilization of Stochastic Nonlinear Systems Subject to Full-State Constraints and Input Saturation," *IEEE Trans. Autom. Control*, vol. 66, no. 3, pp. 1306-1313, Mar. 2021.

[22] A. Polyakov, D. Efimov, and W. Perruquetti, "Finite-time and fixed-time stabilization: Implicit Lyapunov function approach," *Automatica*, vol. 51 pp. 332-340, Jan. 2015.

[23] Y. Yao, J. Tan, J. Wu and X. Zhang, "A Unified Fuzzy Control Approach for Stochastic High-Order Nonlinear Systems With or Without State Constraints," *IEEE Trans. Fuzzy Syst*., vol. 30, no. 10, pp. 4530-4540, Oct. 2022.

[24] H. Min, S. Xu, B. Zhang, Q. Ma and D. Yuan, "Fixed-Time Lyapunov Criteria and State-Feedback Controller Design for Stochastic Nonlinear Systems," *IEEE/CAA J. Autom. Sin*., vol. 9, no. 6, pp. 1005-1014, Jun. 2022.

[25] K. Li, Y. Li and G. Zong, "Adaptive Fuzzy Fixed-Time Decentralized Control for Stochastic Nonlinear Systems," *IEEE Trans. Fuzzy Syst*., vol. 29, no. 11, pp. 3428-3440, Nov. 2021.

[26] Y. Yao, J. Tan, J. Wu, and X. Zhang, "Event-triggered fixed-time adaptive fuzzy control for state-constrained stochastic nonlinear systems without feasibility conditions," *Nonlinear Dyn*., vol. 105, no. 1, pp. 403-416, Jul. 2021.

[27] C. Bechlioulis and G. Rovithakis, "Robust Adaptive Control of Feedback Linearizable MIMO Nonlinear Systems With Prescribed Performance," *IEEE Trans. Autom. Control*, vol. 53, no. 9, pp. 2090-2099, Oct. 2008.

[28] X. Shao, Y. Shi and W. Zhang, "Input-and-Measurement Event-Triggered Output-Feedback Chattering Reduction Control for MEMS Gyroscopes," *IEEE Trans. Syst. Man Cybern. Syst*., vol. 52, no. 9, pp. 5579-5590, Sep. 2022.

[29] R. Zhang, B. Xu, and W. Zhao, "Finite-time prescribed performance control of MEMS gyroscopes," *Nonlinear Dyn*., vol. 101, no. 4, pp. 2223-2234, Sep. 2020.

[30] X. Shao, H. Si, and W. Zhang, "Fuzzy wavelet neural control with improved prescribed performance for MEMS gyroscope subject to input quantization," *Fuzzy Sets Syst*., vol. 411, pp. 136-154, May. 2021.

[31] X. Bu, C. Hua, M. Lv and Z. Wu, "Flight Control of Waverider Vehicles With Fragility-Avoidance Prescribed Performance," *IEEE Trans. Aerosp. Electron. Syst*., vol. 59, no. 5, pp. 5248-5261, Oct. 2023.

[32] Y. Shi, X. Shao, and W. Zhang, "Neural observer-based quantized output feedback control for MEMS gyroscopes with guaranteed transient performance," *Aerosp. Sci. Technol*., vol. 105, no. 106055, Oct. 2020.

[33] X. Shao, Y. Shi, W. Zhang and H. Cao, "Neurodynamic Approximation-Based Quantized Control With Improved Transient Performances for Microelectromechanical System Gyroscopes: Theory and Experimental Results," *IEEE Trans. Ind. Electron*., vol. 68, no. 10, pp. 9972-9983, Oct. 2021.

[34] L. Chen, H. Liang, Y. Pan and T. Li, "Human-in-The-Loop Consensus Tracking Control for UAV Systems Via an Improved Prescribed Performance Approach," *IEEE Trans. Aerosp. Electron. Syst*., doi: 10.1109/TAES.2023.3304283.

[35] H. Xu, D. Yu and Y. Liu, "Observer-Based Fuzzy Adaptive Predefined Time Control for Uncertain Nonlinear Systems with Full-State Error Constraints," *IEEE Trans. Fuzzy Syst*., doi: 10.1109/TFUZZ.2023.3321669.

[36] S. Sui, C. Chen and S. Tong, "A Novel Full Errors Fixed-Time Control for Constraint Nonlinear Systems," *IEEE Trans. Autom. Control*, vol. 68, no. 4, pp. 2568-2575, Apr. 2023.

[37] X. Guo, X. Fan and C. Ahn, "Adaptive Event-Triggered Fault Detection for Interval Type-2 T–S Fuzzy Systems With Sensor Saturation," *IEEE Trans. Fuzzy Syst*., vol. 29, no. 8, pp. 2310-2321, Aug. 2021.

[38] J. Farrell, M. Polycarpou, M. Sharma and W. Dong, "Command Filtered Backstepping," *IEEE Trans. Autom. Control*, vol. 54, no. 6, pp. 1391-1395, Jun. 2009.

[39] W. Dong, J. Farrell, M. Polycarpou, V. Djapic and M. Sharma, "Command Filtered Adaptive Backstepping," *IEEE Trans. Control Syst. Technol*., vol. 20, no. 3, pp. 566-580, May. 2012.

[40] Y. Li, "Command Filter Adaptive Asymptotic Tracking of Uncertain Nonlinear Systems With Time-Varying Parameters and Disturbances," *IEEE Trans. Autom. Control*, vol. 67, no. 6, pp. 2973-2980, Jun. 2022.

[41] L. Wang, H. Wang, P. Liu, S. Ling and S. Liu, "Fuzzy Finite-Time Command Filtering Output Feedback Control of Nonlinear Systems," *IEEE Trans. Fuzzy Syst*., vol. 30, no. 1, pp. 97-107, Jan. 2022.

[42] Y. Yao, J. Tan, J. Wu, X. Zhang, and L. He, "Prescribed tracking error fixed-time control of stochastic nonlinear systems," Chaos Solitons Fractals, vol. 160, no. 112288, Jul. 2022.

[43] Z. Xu, B. Xi, G. Yi, and C. Ahn, "High-precision control scheme for hemispherical resonator gyroscopes with application to aerospace navigation systems," *Aerosp. Sci. Technol*., vol. 119, no. 107168, Dec. 2021.

[44] C. Li, Y. Wang, C. Ahn, C. Zhang and B. Wang, "Milli-Hertz Frequency Tuning Architecture Toward High Repeatable Micromachined Axi-Symmetry Gyroscopes," *IEEE Trans. Ind. Electron*., vol. 70, no. 6, pp. 6425-6434, Jun. 2023.

[45] M. Wang, H. Liang, Y. Pan and X. Xie, "A New Privacy Preservation Mechanism and a Gain Iterative Disturbance Observer for Multiagent Systems," *IEEE Trans. Netw. Sci. Eng*., doi: 10.1109/TNSE.2023.3299614.

[46] X. Wu, K. Xu, and X. He, "Disturbance-observer-based nonlinear control for overhead cranes subject to uncertain disturbances," *Mech. Syst. Signal Process*., vol. 139, no. 106631, May. 2020.

[47] S. Qasem, A. Ahmadian, A. Mohammadzadeh, S. Rathinasamy, and B. Pahlevanzadeh, "A type-3 logic fuzzy system: Optimized by a correntropy based Kalman filter with adaptive fuzzy kernel size," *Inf. Sci*., vol. 572 pp. 424-443, Sep. 2021.

[48] R. Zhang, B. Xu and P. Shi, "Output Feedback Control of Micromechanical Gyroscopes Using Neural Networks and Disturbance Observer," *IEEE Trans. Neural Netw. Learn. Syst*., vol. 33, no. 3, pp. 962-972, Mar. 2022.

[49] R. Zhang, B. Xu, Q. Wei, T. Yang, W. Zhao and P. Zhang, "Serial-Parallel Estimation Model-Based Sliding Mode Control of MEMS Gyroscopes," *IEEE Trans. Syst. Man Cybern. Syst*., vol. 51, no. 12, pp. 7764-7775, Dec. 2021.

[50] M. Basin, P. Yu, and Y. Shtessel, "Finite- and fixed-time differentiators utilising HOSM techniques," *IET Contr. Theory Appl*., vol. 11, no. 8, pp. 1144-1152, May 2017.